63-2-4

AFCRL - 62 - 311

296231

EFFECTS OF THE ATMOSPHERE ON RADIO ASTRONOMICAL SIGNALS

by Robert Fleischer, Masakazu Oshima,
Terry P. Roark, Ronald M. Straka,
and Marvin DeJong

Rensselaer Polytechnic Institute
Troy, New York

Final Report

Prepared

for

EFFECTS OF THE ATMOSPHERE ON RADIO ASTRONOMICAL SIGNALS

by Robert Fleischer, Masakazu Oshima,
Terry P. Roark, Ronald M. Straka,
and Marvin DeJong

Rensselaer Polytechnic Institute
Troy, New York

Final Report

Prepared

for

Requests for additional copies by Agencies of the Department of Defense, their contractors and other Government agencies should be directed to the:

ARMED SERVICES TECHNICAL INFORMATION AGENCY
ARLINGTON HALL STATION
ARLINGTON 12, VIRGINIA

Department of Defense contractors must be established for ASTIA services or have their need-to-know certified by the cognizant military agency of their project or contract.

All other persons and organizations should apply to the:

U. S. DEPARTMENT OF COMMERCE
OFFICE OF TECHNICAL SERVICES
WASHINGTON 25, D. C.

Abstract

Observations of the apparent temperature of thunderstorm cells were made at a number of frequencies, from 10 cps to 3000 Mc during the month of July 1961. The storm July 21 is analyzed in detail. The observations are summarized in section 2.

Section 3, 4, and 5 develop a theory to predict the antenna temperature T_A which may be expected from a storm cell. Briefly, the optical depth of the storm cell and the surrounding atmosphere is found to be low. Emission of radiation apart from sudden lightning discharges is attributed to corona discharge from charged particles within the storm cell. The discharges are assumed to be similar in character to the point-to-plate discharges studied in the laboratory, which are characterized by pulses.

Section 6 gives the calculations of the observed antenna temperature at several frequencies, and section 7 puts limits on the parameters of the discharge model to fit the observations. Section 8 contains a discussion of the extent of agreement of theory and observation with some suggestions for further detail in investigation.

Sections 9 and 10 discuss some precautions which should be taken in future experiments to secure more valid data.

Table of Contents

1. Introduction

The primary emphasis of the contract as it developed was placed on
the determination of the emission of radio frequency radiation by a
thunderstorm cell. The emission of which we speak in this report is the
background, or time-wise continuous emission, not including the impulsive
strokes usually associated with lightning discharges.

In subsequent sections of this report we describe the determination
of antenna temperatures during the storm of July 21, 1961 with the radio
astronomy equipment of the Sagamore Hill Observatory, and the gathering of
other relevant meteorological data. An equation of transfer is set up to
represent the passage of radiation through the storm cell. The source of
radio frequency radiation within the cell is assumed to be corona discharge
from charged droplets in the cloud, and on this basis a prediction of the
variation of antenna temperature with frequency is obtained.

In addition to the primary emphasis on the thunderstorm activity,
the following investigations were pursued at the Sampson Station of the
Observatory of RPI. A continual monitoring, with only moderate
interruptions for equipment servicing and repair, has been made of the
following parameters:

> 18-megacycle cosmic-noise intensity,
> Atmospheric electric potential gradient,
> Intensity of reflected light from the northern sky,
> Atmospheric pressure fluctuation with a microbarovariograph.

The immediate objective of the monitoring tabulated above was to find
examples of tropospheric effects on the transmission of 18-megacycle
cosmic noise, and to evaluate the relationships between the absorption of
this noise and the other parameters. Additionally, the relationship
between atmospheric electric potential gradient and the intensity of
reflected light, together with standard weather information, should help
to indicate the electrical properties of specific storm centers, and is
related to the main thunderstorm project. The records which were
assembled have been maintained in good form on the campus of RPI in Troy.

A patrol of the sun with the 517-megacycle swept-lobe interferometer at the Sampson Station, designed to measure the angular positions and motions of sources of solar radio bursts, has brought to light some fluctuations of atomspheric noise level at that frequency, in addition to the effects of lightening discharges.

Two additional programs at Sagamore Hill were as follows:

(1) On about 15 mornings during July sea-interferometer patterns were observed for the rising sun at L and S bands by Roark (RPI) and Straka (AFCRL). These data are intended to be reduced to further test the hypothesis that atmospheric blobs produce sunrise scintillations. Only preliminary reductions have been made so far, and no conclusions have yet been reached.

(2) An effort to locate Comet Wilson at 2945 Mc was made by Straka and Roark on July 26 through 29. Correlation with results from a similar effort at Harvard initially pointed to a successful detection at this frequency, but subsequently it was decided that the observed results were due primarily to equipment instabilities.

2. Description of Observations

Efforts to observe possible radio-frequency emission from thunderstorm cells were concentrated during the month of July, 1961. There was a moderate number of violent tropospheric storms during this period, most of which were observed.

When a thunderstorm cell was sighted by the radar equipment at Blue Hill its position was communicated to the observers at Sagamore Hill. New altitude-azimuth coordinates for Sagamore Hill were computed and then converted to hour angle and declination for use with the 84-foot paraboloid antenna. This coordinate conversion process took only a few minutes as extensive use was made of pre-calculated tables. Thus, the observers were able to locate the cell before it had a chance to radically shift its position as found by Blue Hill. Upon location of a cell, it would be observed for varying amounts of time with all equipment then operable.

The observations of the July 21, 1961 storm, which was observed from 1400 EST to 1700 EST, are the most complete and our analysis is concentrated on this event. The instrument outputs display no atypical traces and therefore this storm can be used as a general case.

On this date, two violent weather fronts containing high winds, hail, thunderstorm cells and precipitation were in the vicinity of the AFCRL Sagamore Hill Radio Astronomy Observatory near Hamilton, Massachusetts. One of these fronts had already passed through the area and was to the south of the observatory. The other, which was the one observed, was to the north-northwest and traveling in a south-southeasterly direction at a mean azimuth of 300 degrees reckoned from the Sagamore Hill site, assuming zero degrees azimuth to the North. This movement is shown quite clearly (Figure 2-1) on plots of radar data from the Blue Hill, Massachusetts, Meteorological Observatory. The radar observations show a group of cells about 15 miles to the north-northwest of Sagamore Hill at 1543 EST on this date. A later radar observation of the same cells, made 1719 EST, shows their position to be nearly over the Sagamore Hill site.

No precipitation was recorded at Sagamore Hill during the times of observation at 200 Mc and above. At approximately 1825 EST a shift of wind direction at the site indicated the passage of the observed front. Rain commenced at the site at this time. The temperature of the cell at low frequencies (5 to 30 Mc) was measured at this later time.

The observations available for the July 21 activity are summarized below.

a). 10 cycles per second to 9000 cycles per second

These data were taken by a swept frequency receiver under the operation of Mr. William Barron of AFCRL. The antenna was relatively non-directional. The record for this date shown in Figure 2-2, shows a marked widening of the recorder trace which can perhaps be attributed to the effect of numerous lightning strokes. The general level, though, is not rasied to any appreciable extent. The widening effect is particularly noticeable at the lower and higher end of the frequency range swept by this instrument. The mid-range seems relatively unaffected.

b). 5 Megacycles per second

The antenna for this frequency is a long wire with a broad directivity to the north. The record for July 21, shown in Figure 2-3, exhibits a general rise in the intensity base level centered about 1800 UT. It is felt that the lightning-originated bursts were not the primary cause of the general rise in level. The burst number during the 1830 to 1900 UT time interval was as large or larger with little resultant change to the base level.

Sagamore
Hill

Figure 2-1

Thunderstorm Cell Positions, July 21, 1961

⬤ ----- 1543 EST

▨ ----- 1719 EST

60 cps

← FREQUENCY   1600 EST

60 cps

← TIME   1600 EST
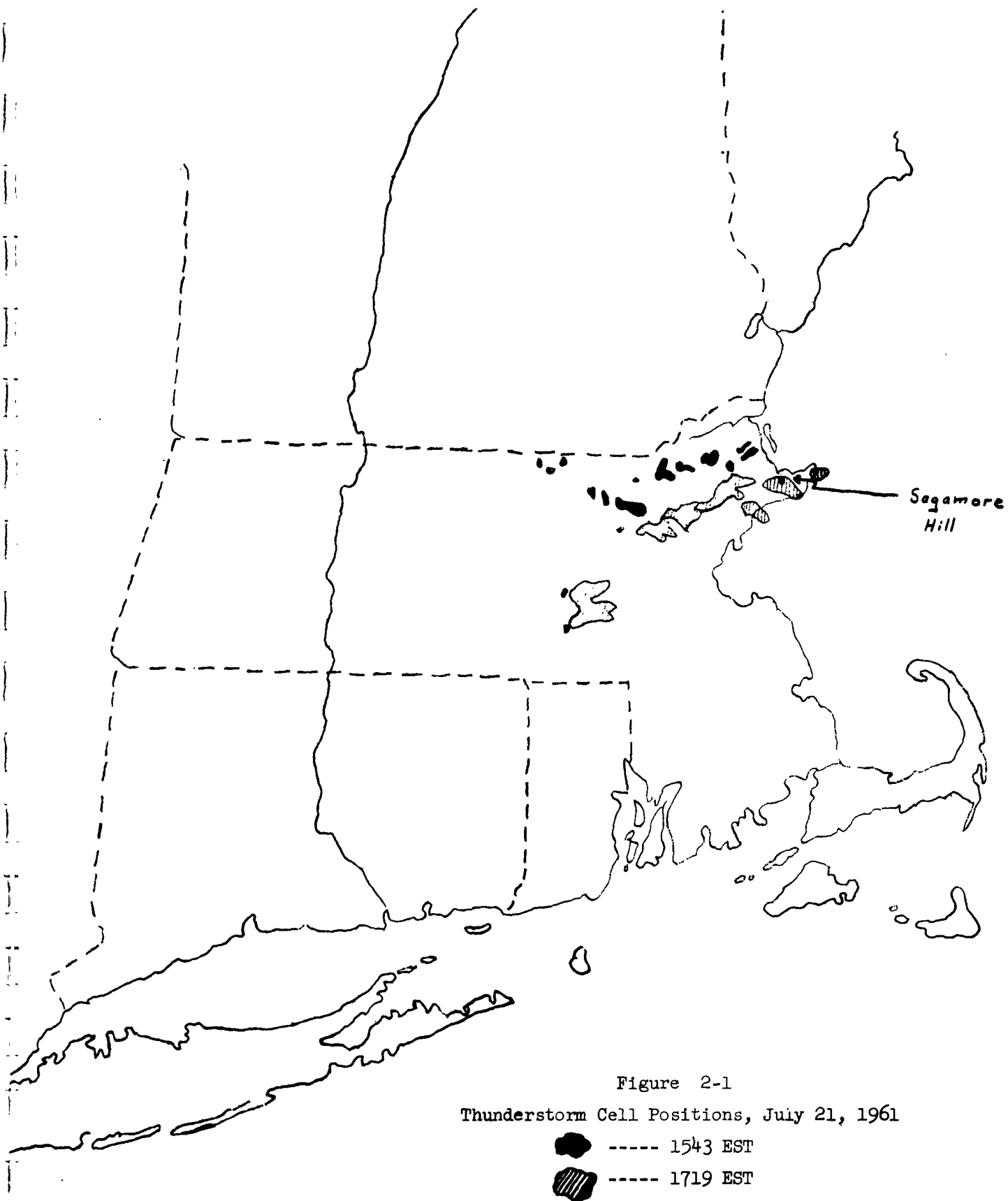
Figure 2-2. 10 to 9000 cps Data

Two Sweeps - 10 to 900 cps and 800 to 9000 cps

Total Sweep Length: 44 Minutes, 54 Seconds

Top - Monday, July 17, 1961 (No Storm)

Bottom - Friday, July 21, 1961 (Severe Storm)

Figure 2-3. 5 Mc/s Radiometer Data
Top – Monday, July 17, 1961 (Moderate Storm)
Bottom – Friday, July 21, 1961 (Severe Storm)

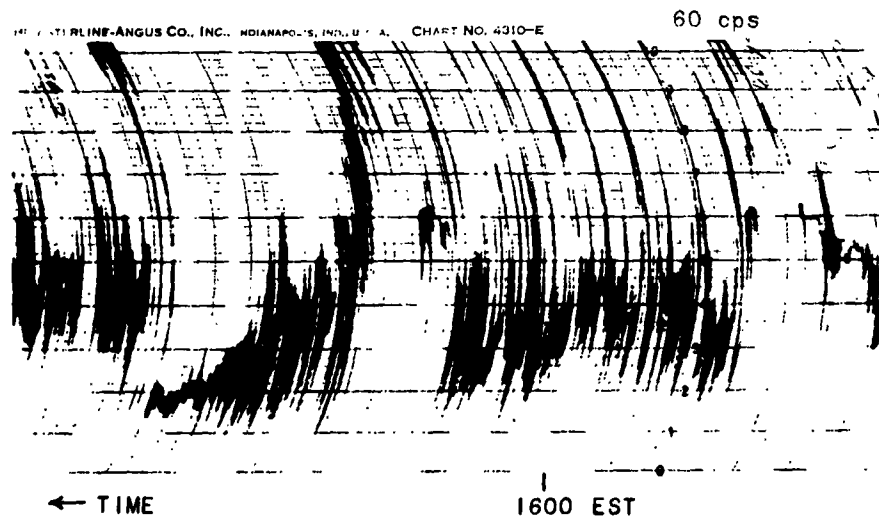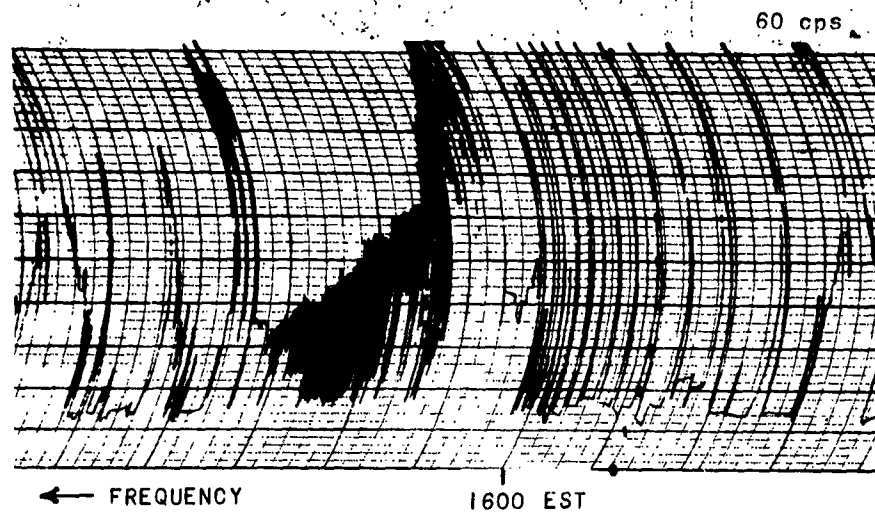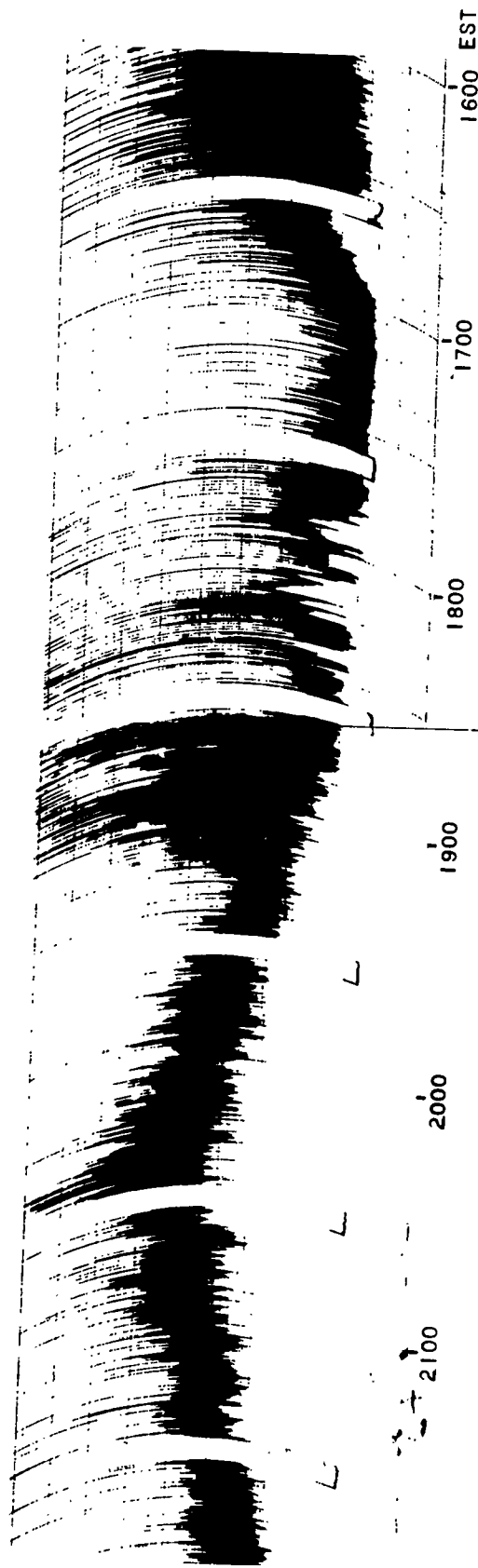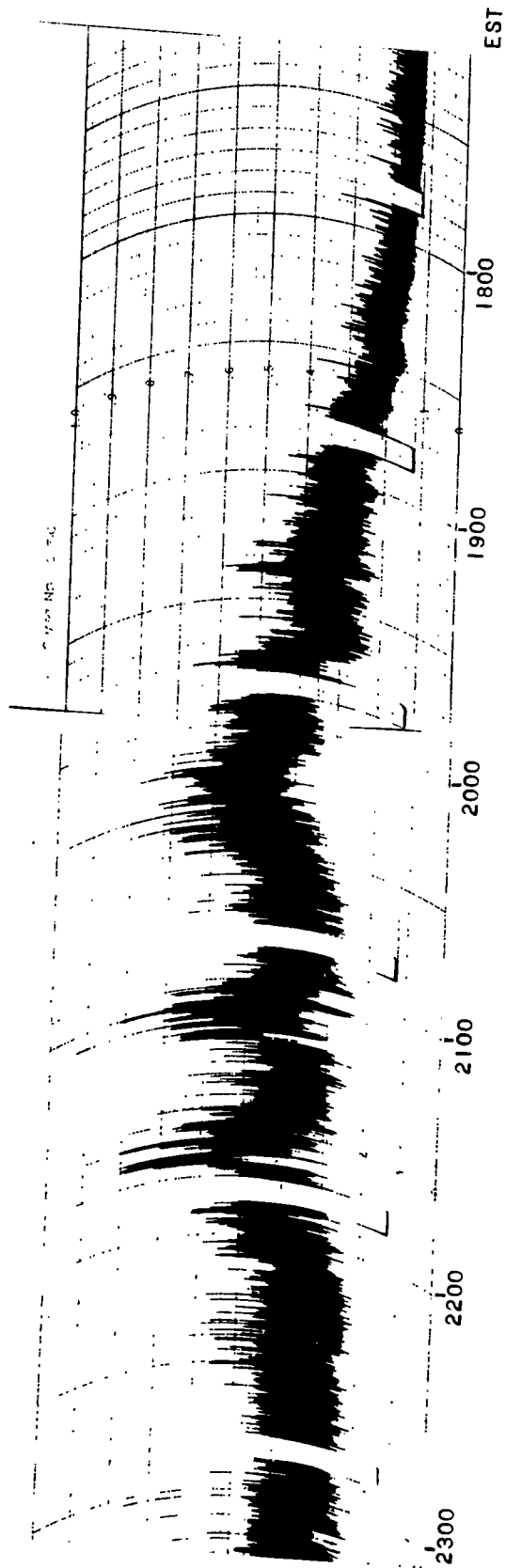Several interesting characteristics are displayed on the 5 Mc record for this date. A small general rise in noise level began about 1200 EST and reached its maximum value at 1640 EST whereupon a sudden drop in noise intensity occurred with the trace reaching normal matched-load level by 1700 EST. Ignoring some short-lived fluctuations, a second general rise began about 1800 EST, reaching a larger maximum value at about 2040 EST as compared to the previous maximum and falling to matched-load level at a rate quite similar to the rise rate. The sudden drop in noise level before 1700 was not repeated after 2040 EST.

The storm cells observed at higher frequencies by the directional antenna at 1615 EST were to the north-northwest of Sagamore Hill and had not passed over the station though disturbed weather conditions were present at the Hill. These may have caused the preliminary 5 Mc rise before 1640 EST. The passage over the site of the actual squall line associated with the cells could then account for the very large maximum observed at 2040 EST.

These records are shown in Figure 2-3 with a relatively quiet day for comparison. Note the normal daily rise in noise level from 1800 to 2015 EST.

c). 10 Megacycle per second

This radiometer has a half wavelength, fifty ohm impedence, dipole antenna well above the ground to minimize ground effects.

Two general rises were also observed on this frequency which were analogous to the 5 Mc data presentation. However, the rapid drop in noise intensity exhibited by the 5 Mc observations at 1640 EST was not in evidence at 10 Mc. The 10 Mc data is most difficult to analyze in this qualitative manner as the recorder tracings fluctuate wildly throughout the first rise and drop in noise level. It would be most difficult to ascertain the time corresponding to the first peak value as the trace goes completely and consistently off scale in both directions. Fortunately the second maximum is somewhat easier to determine. This occurred at about 2040 EST and correlates well with the 5 Mc data.

As before, we are assuming the rise in level is not due to the super-position of successive lightning strokes.

d). 30 Megacycles per second

The 30 Mc riometer was connected to a three element yagi antenna pointed toward the north polar region of the celestial sphere.

Between 1200 EST and 2100 EST these records exhibit extremely noisy conditions; much more so than even the noisiest periods for three days before and after July 21, 1961. A maximum occurs about 1615 EST. See Figure 2-4. No well defined second maximum shows as observed on 5 Mc and 10 Mc. This equipment was under the direction of Mr. H. Strick, AFCRL.

e). 220, 1200, and 3000 Megacycles per second

These three frequencies will be discussed together since they shared a common antenna and their behavior exhibits similar aspects. The antenna used was the AFCRL 84-foot equatorial mounted paraboloid with a Jasik feed for simultaneous reception of the 220, 1200, and 3000 Mc radiation.

During the course of the afternoon several cells were observed. However, the particular one denoted γ, at azimuth 293° from Sagamore Hill, altitude 7° 45', 1615 EST is the one which will be discussed in detail. The recorder trace of the noise level shows a marked increase in intensity on all these frequencies as the antenna is pointed nearer to the cell. Individual lightning strokes are fairly prevalent at 220 Mc with fewer at 1200 Mc and almost none at 3000 Mc.

f). Other sources of data

Several other sources of data were available and many have been included in the discussion above. These include:

1). Wind direction and speed at Sagamore Hill.

2). Temperature recordings at Sagamore Hill.

3). Local area weather condition reports collected from a group of observers by Mr. Pat Harney, AFCRL Meteorological Development Laboratory.
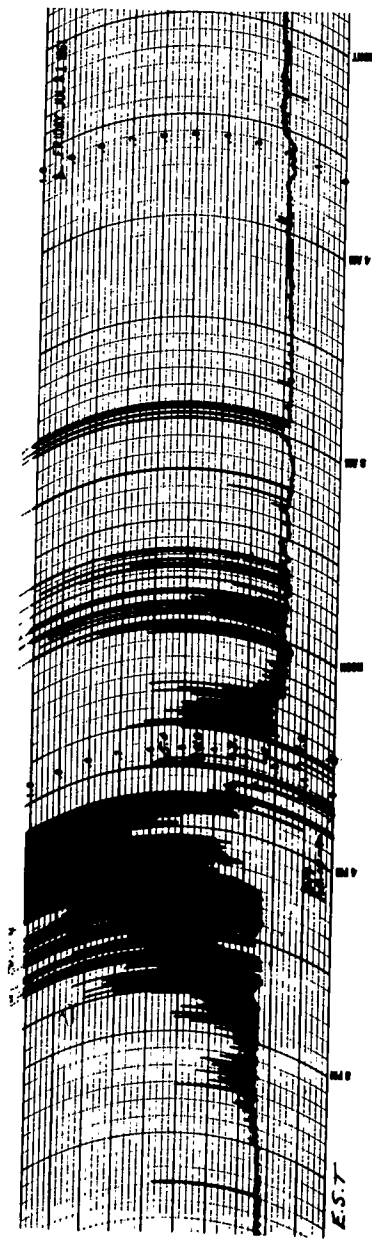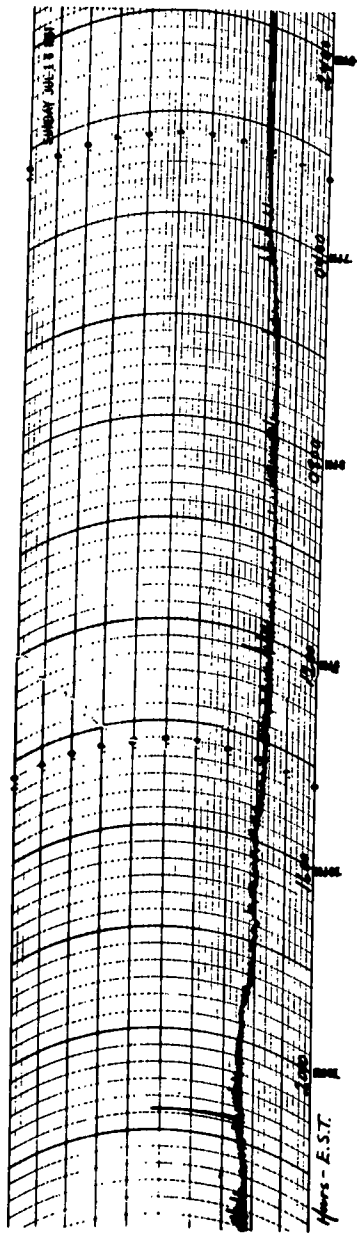
Figure 2-4. 30 Mc/s Riometer Data

Top - Sunday, July 16, 1961 (NO Storm)

Bottom - Friday, July 21, 1961 (Storm)
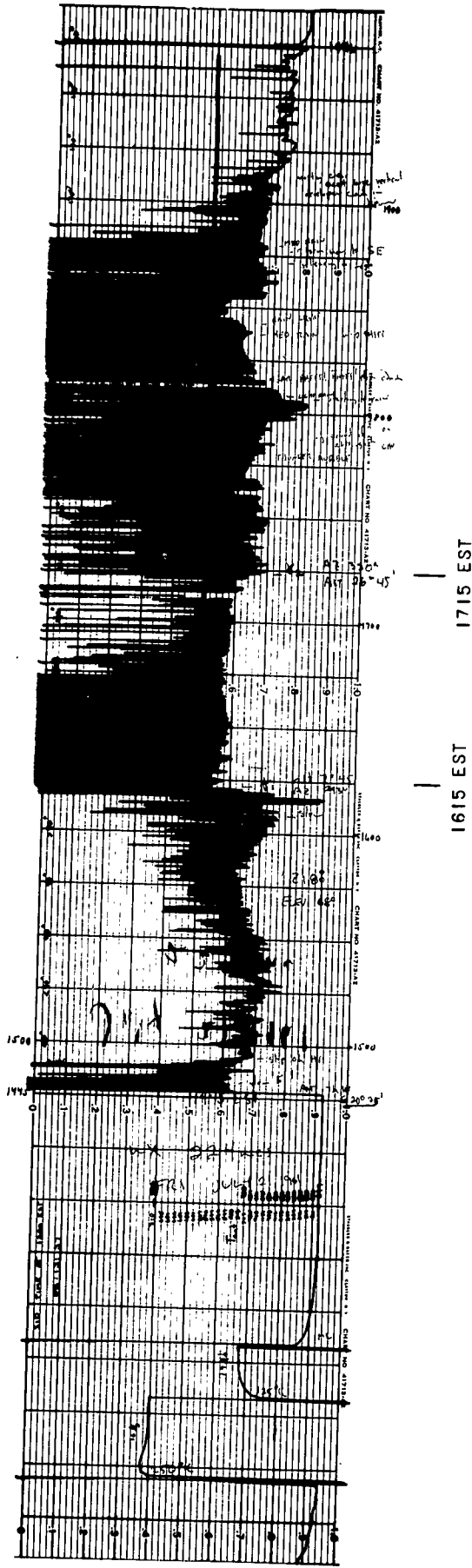
1615 EST   1715 EST

FIGURE 2-5   224 Mc/s RADIOMETER DATA

for the storm of July 21, 1961. At 1615 EST the antenna was pointed toward cell γ_1.

At 1715 EST the antenna was moved off γ_1 to another cell γ_2.

4). United States Weather Bureau facsimile maps of weather conditions in the immediate and surrounding area.

5). Radar determinations of thunderstorm cell location and their profiles taken by the Weather Radar Branch, Meteorological Research Laboratory, AFCRL.

6). Sferic Location data, from the Air Weather Service Reporting Network, which also indicates the positions of local thunderstorm cells.

7). Backscatter data from the ionosphere at 19.4 Mc taken near Ipswich, Massachusetts, by Mr. Chet Malik, AFCRL.

8). Ionosphere soundings taken at Millstone Hill, Massachusetts, by Dr. W. W. Smith, M.I.T. Lincoln Laboratory.

It should be noted that on July 21, 1961, there was no backscatter to the north during the period of intense storm activity. This is rather an anomalous situation from that observed for the preceding and following few days. The night of the 21st, diffuse F and aurorae were observed. Also, a sudden cosmic noise absorption of importance 1 was observed about 1203 EST as reported in the National Bureau of Standards publication of Solar Geophysica' Data issued November 1961, but this same event was not observed on the 18 Mc equipment operated by Rensselaer near Grafton, New York.

No effects of the July 21 storm showed on the records obtained at Grafton, although there were some periods of atmospheric electrical activity during the day. We assume these latter to be related to local atmospheric phenomena not directly connected with the storm cells observed from Sagamore Hill.

3. The Predicted Antenna Temperature Due to a Storm Cell.

We assume for the present that the optical depth of the atmosphere outside the storm cell is negligible. In general the antenna temperature T_A will be (when the cell fills the beam)

$$T_A = T_b(1-e^{-\tau}) + T_{sky}e^{-\tau} \qquad (3\text{-}1)$$

where T_b is the brightness temperature of the storm cell, τ is the optical depth of the cell, and T_{sky} is the brightness temperature of the distant sky background (atmosphere, ionosphere or galaxy, depending on the frequency). See Figure 3-1a. The effect of the presence of a storm will be to change the first term from zero, with a corresponding change of T_A.

T_b is related to the brightness b of the storm cell by the following well-known equation (Pawsey and Bracewell, page 15, eqn 7):

$$b = \frac{2kT_b}{\lambda^2} = 2.77 \times 10^{-23} \frac{T_b}{\lambda^2} \qquad \text{watt m}^{-2} \text{ (c/s)}^{-1} \text{ steradian}^{-1} \qquad (3\text{-}2)$$

Thus we must predict b in order to find T_b.

Assume there to be n particles per unit volume each emitting ε watts per (cycle / sec) bandwidth at the frequency of observation. We call ε the emission coefficient per particle. n and ε may be evaluated for each emission process envisioned; we are interested in the sum $\Sigma n\varepsilon$. Assuming the emission to be isotropic, then each unit volume emits

$$\frac{n\varepsilon}{4\pi} \qquad \text{watts (c/s)}^{-1} \text{ steradian}^{-1} \qquad (3\text{-}3)$$

in our direction. The total emission in the direction of the antenna will be the above number multiplied by the volume of the storm cell which we will call V. Consider this volume to be the product of the surface area A times the thickness of the cell x, measured along the line of sight. Then the brightness of the storm cell is

$$b = \frac{Vn\varepsilon}{4\pi A} \qquad (3\text{-}4)$$

or, $\qquad b = \frac{n\varepsilon x}{4\pi} \qquad \text{watts (c/s)}^{-1} \text{ steradian}^{-1} \qquad (3\text{-}5)$

Substituting equation (2), we have for the brightness temperature of the storm cell

$$T_b = \frac{\lambda^2 b}{2.77 \times 10^{-23}} = \frac{\lambda^2 Vn\varepsilon}{4\pi A(2.77 \times 10^{-23})} \qquad (3\text{-}6)$$

or $\qquad T_b = \frac{\lambda^2 n\varepsilon x}{4\pi(2.77 \times 10^{-23})} \qquad (3\text{-}7)$
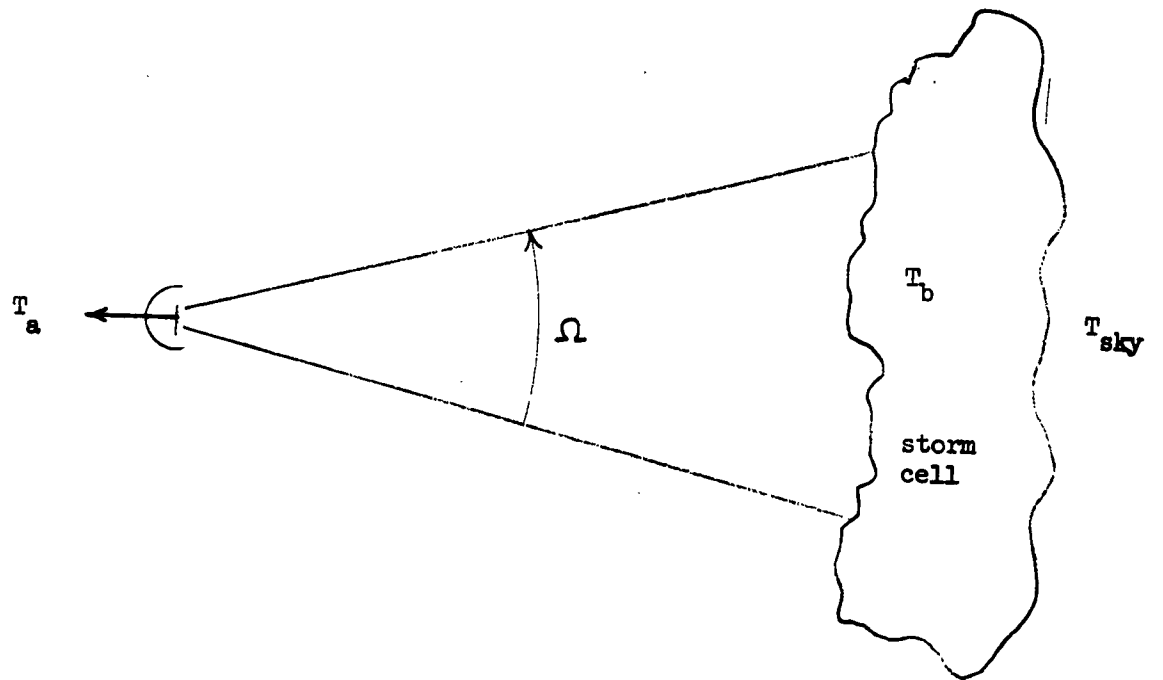
Figure 3-1a
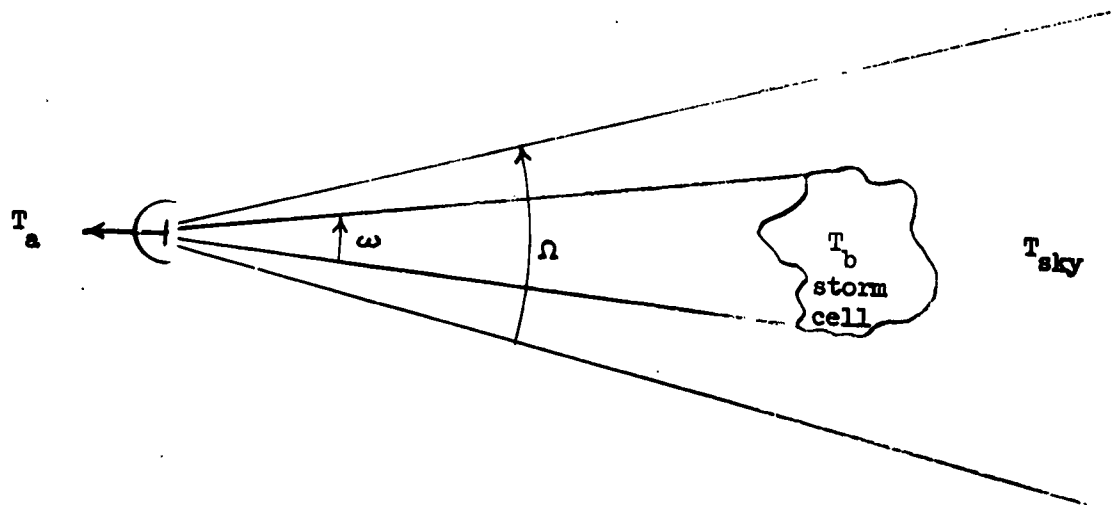
Figure 3-1b

Now we have evaluated one of the quantities, T_b , appearing in equation (3-1). The optical depth τ is simply

$$\tau = \int_0^x k \, dx \qquad (3-8)$$

k being the linear absorption coefficient, and x the thickness of the cell as before.

If the cell does not fill the beam, T_A will be reduced by the ratio of ω to Ω , ω being the solid angle subtended by the cell and Ω being the solid angle of the antenna beam. The first term of (3-1) will become

$$\frac{\omega \lambda^2 n \, \epsilon \, x}{4\pi \Omega 2.77 \times 10^{-23}} (1 - e^{-\tau}) \quad \text{mks units.} \qquad (3-9)$$

The second term of (3-1) becomes in this case $(\omega < \Omega)$

$$T_{sky}(1 - \frac{\omega}{\Omega} + \frac{\omega}{\Omega} e^{-\tau}) \qquad (3-10)$$

See Figure 3-1b.

To predict T_A, we evaluate τ in the next section, Section 4, and ϵ in Section 5.

4. The Optical Depth of the Storm Cell

a). Attenuation Due to Oxygen and Water Vapor

Molecules of oxygen and water vapor provide the principal sources of microwave absorption in the normal atmosphere. Van Vleck (1947) investigated these properties and found that oxygen molecular absorption was quite important in the 4 to 6 mm wavelength range, but of relatively little importance at wavelengths greater then 10 cm. No observations at wavelengths shorter than 10 cm were made in the current investigations, hence we may disregard molecular absorption by oxygen.

Hogg and Mumford (1960) show results indicating that for a water vapor content of one percent in the air we may neglect the effects of water vapor at the frequencies applicable to this investigation. Thus we will assume that the absorption coefficient for normal atmospheric conditions in front of the emitting cell is negligible.

However, within the cloud surrounding the storm cell normal atmospheric conditions are not present. In particular, the water vapor content is much more than 1%. Generally, the attenuation must be expressed as a combination of absorption and scattering by the particles involved. When one considers clouds, however, these droplets are so small as to make scattering quite negligible for our radio frequencies. The absorption can be expressed as a function only of the mass of the condensed water vapor per unit volume, M, the imaginary part of the index of refraction, m, and the wavelength of the incident radiation, λ. Johnson (1955) has tabulated the two-way attenuation per unit mass of cloud as a function of temperature. The maximum values occur at 1.25 cm wavelength and decrease with increasing wavelength. At 10 cm the data show the maximum values:

$$\frac{\gamma}{m} = 0.047 \; \frac{db}{mile} \; \frac{cm^3}{gm} \qquad \text{(Water cloud at -8}^{\circ}\text{ C)}$$

$$\frac{\gamma}{m} = 0.003 \; \frac{db}{mile} \; \frac{cm^3}{gm} \qquad \text{(Ice cloud at 0}^{\circ}\text{ C)}$$

where γ is the logarithmic absorption coefficient per mile.

A typical value for the water-vapor content of nonprecipitating clouds may be as high as 1 gm/cm^3 at the upper levels (Johnson 1954). Inserting this value for m and dividing by 2 to get one-way logarithmic attenuation coefficient per mile the following are obtained:

$$\text{water} = 2.35 \times 10^{-2} \text{ db/mile},$$
$$\text{ice} = 1.5 \times 10^{-3} \text{ db/mile}.$$

Conversion of miles to kilometers yields

$$\text{water} = 1.47 \times 10^{-2} \text{ db/km}$$
$$\text{ice} = 0.94 \times 10^{-3} \text{ db/km} \tag{4-1}$$

By definition the attenuation in db is

$$-10 \log (I/I_o) \tag{4-2}$$

where

I = emergent intensity from unit absorbing volume.

I_o = incident intensity upon unit absorbing volume.

The term (4-2) may be written

$$-10 \log e^{-k} = 10 \, \tau \log e$$

but

$$10 \log e = 4$$

Therefore, from equation (3-8)

$$\text{db} = 4\tau = 4kx \tag{4-3}$$

or

$$\frac{\text{db}}{\text{mile}} = \frac{4k}{\text{mile}}$$

thus

$$k = \lambda/4 . \tag{4-4}$$

Hence from (4-1)

$$k_{\text{water}} = 0.37 \times 10^{-2} \text{ km}^{-1}$$
$$k_{\text{ice}} = 0.24 \times 10^{-3} \text{ km}^{-1}. \tag{4-5}$$

Since

$$\tau = k \, x_{\text{total}}$$

and we are assuming a total path length of 10 km, we have

$$\tau \text{ water} = 3.7 \times 10^{-2}$$

and

$$\tau \text{ ice} = 2.4 \times 10^{-3}, \tag{4-7}$$

for the optical depths of the clouds due to nonprecipitable water vapor, at a wavelength of 10 cm. Longer wavelengths will be even less affected.

b). Scattering by Rain Drops and Snow Flakes

It will be assumed that the law of Rayleigh scattering holds for all wavelengths and drop sizes under consideration in this investigation. The criterion is that the diameter of the scattering particle be small as compared to the wavelength of the incident radiation. The scattering cross section per unit volume is then written (Johnson 1955)

$$\eta = \frac{\pi^5}{\lambda^4} \left| \left(\frac{m^2-1}{m^2+2} \right)^2 \right| \sum_i n_i D_i^6 \qquad (4\text{-}8)$$

where

m = complex index of refraction

n_i = number of scatterers of size i per unit of volume

D_i = diameter of the scattering sphere

The quantity $(m^2-1)^2/(m^2+2)^2$ may, for the order of magnitude calculations contained in this section, be considered independent of λ from 3000 Mc to 200 Mc (von Hippel - 1954). Thus we may write

$$\eta \lambda^4 = (\text{constant})(z) \qquad (4\text{-}9)$$

where, according to Johnson (1955), the constant assumes the values

$$\text{constant} = \begin{array}{l} 0.86 \times 10^{-8} \text{ water} \\ 0.18 \times 10^{-8} \text{ ice} \end{array}$$

and $\qquad z = \sum_i n_i D_i^6$

Now, z may be expressed as (Atlas and Marshall 1952)

$$z = 200 \, R^{1.6} \qquad (4\text{-}10)$$

where R is the rainfall rate in mm per hour.

Finally, we may write

$$\eta \lambda^4 \text{ rain} = 1.7 \times 10^{-6} \, R^{1.6} \text{ for rain}$$

and

$$\eta \lambda^4 \text{ snow} = 0.36 \times 10^{-6} \, R^{1.6} \text{ for snow}, \qquad (4\text{-}11)$$

where η is expressed in ft^{-1} and λ in centimeteres.

Assuming λ = 10 cm and R_{rain} = 90 mm/hour; R_{snow} = 10 mm/hour,

then
$$\eta \text{ rain} = \frac{1.7 \times 10^{-6}}{10^{4}} \times 90^{1.6} \quad (\text{ft})^{-1}$$

$$= 2.21 \times 10^{-7} \quad (\text{ft})^{-1}$$

and
$$\eta \text{ snow} = \frac{3.6 \times 10^{-7}}{10^{4}} \times 10^{1.6} \quad (\text{ft})^{-1}$$

$$= 1.41 \times 10^{-8} \quad (\text{ft})^{-1}$$

If we again assume a line of sight thickness of 10 km. for the cloud, and let
$$\tau = \eta \, x \tag{4-12}$$

Then
$$\tau \text{ rain} = 7.07 \times 10^{-3}$$

and
$$\tau \text{ snow} = 4.51 \times 10^{-4} \tag{4-13}$$

are the values of the optical depth due to scattering by rain drops and snow flakes within the cloud.

c). Scattering by Free Electrons

Since large charge separations are present in thunderstorm cells, as indicated by the phenomenon of lightning, the possibility of attenuation of radiation within the cloud by electron scattering should be investigated.

The linear absorption coefficient due to electron scattering is (Lichtenstein 1959)

$$k_{el} = \frac{2\pi e^{2}}{mc} \frac{\nu}{\nu^{2}+(p+p_{L})^{2}} N_{e} \tag{4-14}$$

where
- e = electronic charge
- m = mass of electron
- c = velocity of light in vacuo
- N_{e} = electron density of the cloud (assumed homogeneous)
- ν = collision frequency in the cloud
- p = frequency of incident radiation
- p_{L} = gyro - frequency of the electrons in the cloud

For the frequencies with which we are concerned (200 Mc to 3000 Mc) it will be assumed that $p \gg p_{L}$ and hence the term $(p+p_{L})^{2}$ may be approximated as p^{2}.

The collision frequency ν depends on the velocities of the electrons and their mean free path l_e in the manner

$$\nu = \frac{\bar{v}}{l_e}$$

(4-15)

The mean velocity $\bar{v}$ is the sum of the thermal and small scale turbulent velocities, i. e.

$$\bar{v} = \bar{v}_{thermal} + \bar{v}_{turbulence}$$

(4-16)

The thermal velocity may be found from

$$\bar{v}_{th} = \left(\frac{8k T}{\pi m}\right)^{1/2}$$

(4-17)

where

k = Boltzmann's constant

T = Electron temperature in the cell (assumed homogeneous throughout) the cloud).

To evaluate $\bar{v}_{th}$ the mean temperature will be chosen as $10°$ C or $283°$K. This is probably a fair assumption as the temperature range for summer thunderstorms seems to be about $0°$ to $20°$ C although colder temperatures are not uncommon. Hence

$$\bar{v}_{th} = \left(\frac{8 \times 1.38 \times 10^{-23} \text{ joule} \times 283 \text{ K}}{3.14 \times 9.1 \times 10^{-31} \text{ kg} \quad \text{K}}\right)^{1/2}$$

$$\doteq 10^5 \text{ meters/second}$$

A typical value for the wind current that serves to carry the charged particles from the bottom of the cloud to the top, according to Vonnegut's theory (1954) would be about

$$\bar{v}_{turbulent} \doteq 5 \text{ meters/second}$$

It is obvious that

$$\bar{v}_{th} \gg \bar{v}_{tu}$$

and thus

$$\bar{v} \doteq \bar{v}_{th} = 10^5 \text{ meters/second}$$

(4-18)

The mean free path, l_e, for the Air Force Model Atmosphere (Campen 1960), at a mean height of 5 km is

$$l_e \doteq 10^{-7} \quad \text{meter.} \tag{4-19}$$

Upon substitution of these values we obtain for the collision frequency

$$\nu \doteq 10^{12} \quad \text{sec}^{-1}.$$

Thus it may further be assumed that p is negligible when compared with ν, even at 3000 Mc. The linear absorption equation may now be written as

$$k_{el} \doteq \frac{2\pi e^2 N_e \nu}{mc\nu^2} = \frac{2\pi e^2}{mc\nu} N_e \tag{4-20}$$

Inserting all the known and constant terms we find that

$$k_{el} \doteq 10^{-19} N_e \quad (m^{-1}).$$

Choosing a value of $N_e = 5 \times 10^{10}/m$ (Vonnegut - 1954),

$$k_{el} = 5 \times 10^{-9} \quad (m^{-1}).$$

For $x = 10$ km $= 10^4$ meters, the optical depth due to electron scattering is

$$\tau_{el} = 5 \times 10^{-5} \tag{4-21}$$

d). Discussion

The optical depths may now be tabulated:

Cause	
Normal Atmosphere	0
Water Cloud (absorption)	3.7×10^{-2}
Ice Cloud (absorption)	2.4×10^{-3}
Rain Drops (scattering)	7.1×10^{-3}
Snow Flakes (scattering)	4.5×10^{-4}
Free Electrons (scattering)	5×10^{-5}

These optical depths are much too small to seriously affect the transfer of radiation through the storm center. This is easily seen by considering

$$T = T_o \, e^{-\tau} \tag{4-22}$$

where   T = observed temperature emitted by the cell,

T$_o$ = actual temperature produced by the cell.

For the case of the largest τ, i. e.,

$$\tau = 3.7 \times 10^{-2}$$

we have

$$T = T_o \, e^{-0.037}$$

or

$$T/T_o = e^{-0.037} \doteq 0.97 \doteq 1$$

Hence effectively,

$$T = T_o$$

for all cases of T. (4-23)

5. The Emission by the Storm Cell

Sources of radiation by a storm cell which might be considered are
(a) thermal radiation, (b) short-duration pulses due to lightning or other
sudden discharges over long distance, (c) large scale ordered oscillations
of charge, (d) noise emitted during corona discharge from small charged
particles. The first of these (a) is ruled out by the small optical
depths found in the previous section. We are specifically excluding pulses
of type (b) from consideration in the observations to be discussed later,
because of the time constants of the receivers were short enough that the
base level was not appreciably affected by lightning discharges but the
time constants were not yet short enough to yield information on the
character of the lightning strokes themselves. Charge separation in the
storm cell appears to be reduced by lightning discharges in such a way
that a continued steady noise source would not be maintained by oscillations
of type (c). We are left with (d) as the mechanism to be considered.

The behavior of the corona discharge between a metallic point and a
metallic plate has been investigated by many people (Amin 1954 , English
1948, Heintz 1959, Denholm 1960). Among these there is a deduction by
Heintz of the current wave form using the diffusion equation.

When an electric source is supplied from outside, as in these cases,
the corona discharge consists of a series of pulses distributed more or
less periodically. The very short pulses which appear when the metallic
point is negative are called Trichel Pulses.

An electrified drop will discharge into the surrounding atmosphere or
to the particle which is oppositely charged, when it is charged high enough
to cause breakdown. In a thunderstorm cell it may be supposed that the
discharge, once induced, continues until the drop is in charge equilibrium
with the surrounding air. We assume that this single discharge is of the
same nature as a Trichel pulse in the point to plate discharge.

We will apply to the particle discharge the current wave form which was
introduced by Heintz, as follows:

$$i = \frac{B}{t^{3/2}} e^{-\frac{\tau}{t} - \beta t} \tag{5-1}$$

(for $t > 0$)

In this expression, τ is a measure of the rate of rise and β is a measure of the rate of fall of the pulse waveform. B is a constant proportional to the amplitude of the pulse, and t is the time.

Actual observations of Trichel pulses using a high speed oscilloscope were made by Denholm (1960). Heintz (1959) measured the frequency spectrum and constructed the pulse waveform from this. The two cases are shown in Figure 5-1.

Heintz's values of B, τ, β are as follows

$$B = 2.61 \times 10^{-8} \text{ u A sec}$$
$$\tau = 11.8 \times 10^{-8} \text{ sec}$$
$$\beta = 4.82 \times 10^{-6} \text{ sec}^{-1}$$

For the pulses measured by Denholm much smaller values of τ and β than given by Heintz must be assumed to make expression (5-1) fit the actual observation.

Using the Laplace transform for a real independent parameter a > 0,

$$(t^{-3/2} e^{-a/4t}) e^{-st} dt = 2\pi^{1/2} a^{-1/2} e^{-(ap)^{1/2}}$$

the Fourier transform of (5-1) can be reduced to:

$$I(\omega) = B \frac{\pi}{\tau}^{1/2} \exp\left(-\sqrt{2\tau\left[(\omega^2+\beta^2)^{1/2}+\beta\right]}\right) \tag{5-2}$$

If the discharge distance is assumed to be L, the dipole moment $\hat{P}_1(\omega)$ becomes

$$\left|P_1(\omega)\right| = \left|I(\omega)\right| \times L \tag{5-3}$$

This expression is the Fourier transform of the individual corona discharge, and the radiated power due to this dipole moment becomes:

$$\mathcal{E}(\omega) = \frac{\omega^2}{12\pi}\mu\sqrt{\mu\varepsilon_0}\left|P_1\right|^2 \qquad \text{mks units} \tag{5-4}$$

ma.

10

5

0

0   10

20 X 10^{-8} sec.
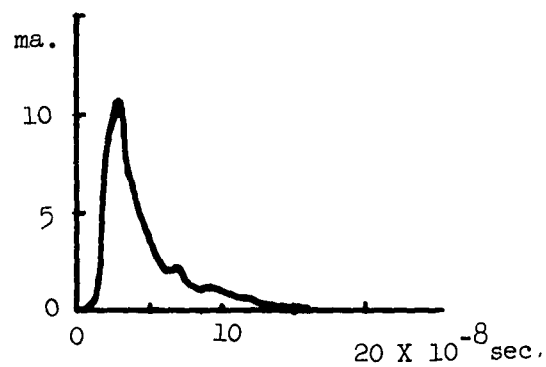
(a).   Pulse shape observed by Denholm.

μa.

200

100

0

0   20   40   60 X 10^{-8} sec.
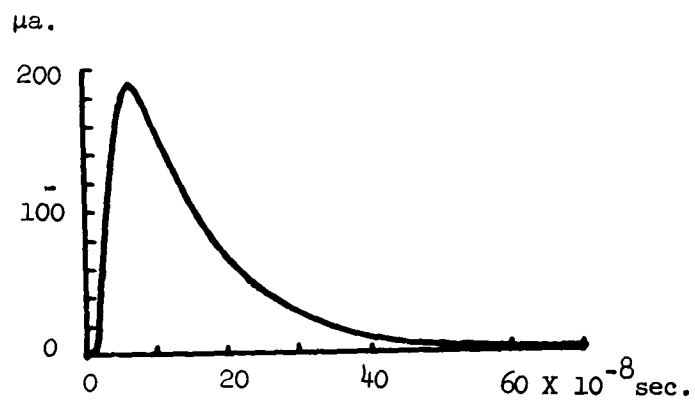
(b).   Pulse shape by Heintz.

Figure 5-1.   Trichel Pulse Shapes.

In the region of the thunderstorm cell where corona discharge is occurring, the average number of discharges per unit volume per second is n, as described in section 3. The direction of the discharge current can be considered to be distributed at random and there is no phase correlation between discharges. Also the intervals between discharges are random.

In this situation, the total radiated power from all the particles becomes

$$W(\omega) = n \ V \ \mathcal{E} \ (\omega) \tag{5-5}$$

We can apply equations (3-4) and (3-6) to find the brightness temperatures. For the surface area in expression (3-4) we take

$$A = \pi R_s^2 \tag{5-6}$$

R_s being the radius of a spherical cell.

The expression (3-6) for T_b then becomes, using (5-4) for $\mathcal{E}$,

$$T_b = \frac{10 \ n \ V \quad P_1^{\ 2}}{2.77 \times 10^{-23} \ R_s^2} \tag{5-7}$$

The factor 10 arises from using the following relations in (3-6):

$$\frac{1}{\sqrt{\mu_0 \epsilon_0}} = c \ \ ; \ \ 2\pi f = \omega$$

and

$$\lambda f = c \ .$$

The frequency dependence of T_b enters through P_1 via-equations (5-3) and (5-2). Inspection of equation (5-4) shows that at lower frequencies $\mathcal{E}$ (ω) increases with ω^2, $I(\omega)$ being constant at the lower frequencies. At higher frequencies, $\mathcal{E}$ (ω) or $W(\omega)$ varies as $\omega^2 \exp \ (-2\sqrt{2\pi\omega})$ and decreases with frequency because of the exponential factor.

Returning to the equation (5-7), T_b will stay constant with frequency until it is depressed by the exponential factor. Numerical estimates are discussed in section 7.

In the above derivation, the effect of the movements of the electrons in the corona discharge was not taken into account. The current in equation (5-1) is the resultant motion of the order of 10^{10} electrons in one discharge. Because the electron collision frequency is of the order of 10^{12} sec^{-1} at atmospheric pressure, and the duration of the corona is of the order of 10^{-7} second, one discharge involves many collisions of electrons and consequently random motion of the electrons inside the corona region superposed on the resultant currents. The radiation due to this random motion of electrons is the same nature as radiation from ionized plasmas and is not taken into account in the above expression. Because of the interval between each collision is very small compared to the duration of the corona discharge, the radiated power spectrum due to each electron step must be displaced into far higher frequency ranges than the radiation due to the resultant discharge current.

The theory outlined above is not suitable for application to emission by lightning. If we were to consider a lightning discharge the time duration would be of the order of milliseconds and the length of the discharge very long, resulting in a large dipole moment. In this case the maximum of the frequency spectrum of the radiated power is displaced downward into the kilocycle range. The extent of the ionized region is also large and the plasma radiation could not be neglected as we have done.

6. Antenna Temperature Calculations for 1961 July 21

a). Calculations at 3000 Mc (S-Band Radiometer)

For the calculation of antenna temperatures an equivalent block diagram is shown in Figure 6-1. In Figure 6-1, α_1 represents the power loss in the transmission line, α_2 the insertion loss of attenuator no. 1, α_3 the coupling factor for the antenna section, α_4 the power loss of attenuator no. 4, α_5 the coupling factor for the noise source section, α_6 the insertion loss of the variable attenuator, and α_A is the power loss supplied by the variable attenuator. T_a is the antenna temperature and T_n is the effective temperature of the noise source which is given as $10,000^\circ K$. Table 6-1 summarizes the available data for the S-Band Radiometer.

Calibration of the receiver proceeds as follows: First the receiver is warmed up and connected to matched load. Matched load consists of inserting a large attenuation in attenuator no. 1. Secondly, the noise source is turned on and several calibration steps are placed on the recorder chart by means of the calibrated variable attenuator no. 3.

When the receiver is connected to matched load it sees a temperature T_1 given by the expression

$$T_1 = T_o(1-\alpha_2)\,\alpha_3\,\alpha_4 + T_o(1-\alpha_3)\,\alpha_4 + T_o\,\alpha_6\,\alpha_a\,\alpha_5\,\alpha_4$$

$$+ T_o\,(1-\alpha_6\,\alpha_a)\,\alpha_5\,\alpha_4 + T_o(1-\alpha_4) \tag{6-1}$$

$$T_1 = 311^\circ K$$

In equation (6-1) T_o is the temperature of the matched load and the room (about $290^\circ K$) and the α's represent the losses of the components in the receiver feed line.
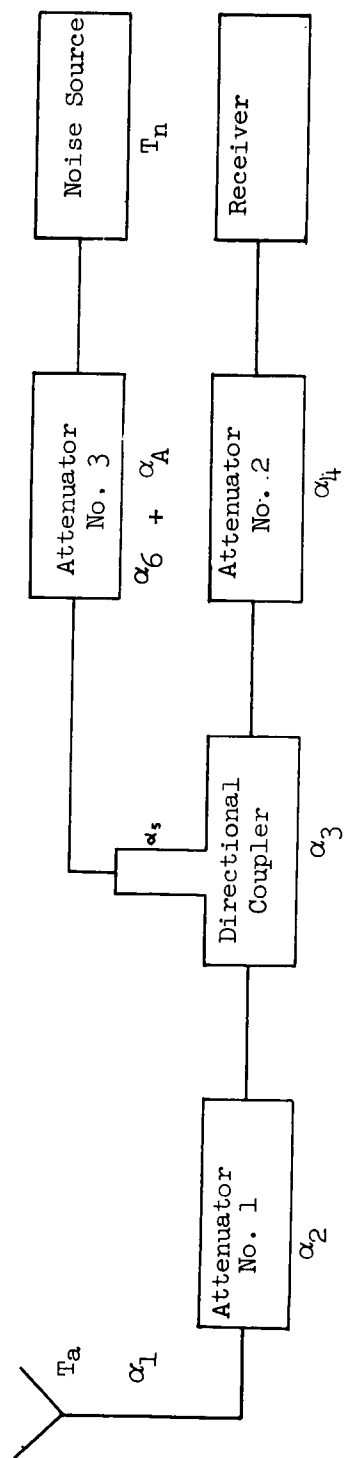
Figure 6-1. Equivalent block diagram of S-Band Radiometer.

Symbol	Decibels	Power ratio
α_1	1.9	.646
α_2	.2	.955
α_3	.1	.977
α_4	.8	.832
α_5	10.5	.089
α_6	.1	.977

Table 6-1. Constants of the receiver

When noise is now introduced the receiver sees a temperature

$$T_2 = \left\{ \left[T_n\alpha_6\alpha_a + T_0(1-\alpha_6\alpha_a) \right] \alpha_5 + T_0 \right\} \alpha_4 + (1-\alpha_4) \, T_0$$

$$T_2 = 702^\circ K \, (\alpha_a) + 311^\circ K \tag{6-2}$$

To calibrate the chart we need only vary α_a by steps, and note the corresponding change on the receiver output record.

Finally to measure the antenna temperature the attenuation in attenuator no. 1 is reduced, i.e. the antenna is turned on, and the noise is brought up to about matched load level by means of variable attenuator no 3. In this case the receiver sees a temperature T_3 given by

$$T_3 = \left\{ \left[T_a\alpha_1\alpha_2\alpha_3 + T_0(1-\alpha_1\alpha_2\alpha_3) \right] + \left[T_n\alpha_a\alpha_6 + T_0(1-\alpha_a\alpha_6) \right] \alpha_5 \right\} \alpha_4$$
$$+ (1-\alpha_4) \, T_0 \tag{6-3}$$

Solving for T_a we find

$$T_a = 2 \left[T_3 - 702^\circ K(\alpha_a) - 166^\circ K \right] \tag{6-4}$$

To obtain the antenna temperature from the chart records we compute T_3 by means of the calibration marks on the chart, use the value of α_a given for the particular measurements, and apply equation (6-4).

On the July 21 record there are two calibration points in addition to the matched load level. For the first calibration point α_a is .020 corresponding to 17 db. in attenuator no. 3. Using equation (6-2) we find that this gives $14^\circ K$ above matched load. The record shows a deflection of 2.1 scale divisions, thus the calibration constant is $6.7^\circ K$ per scale division.

The second calibration point on the record is obtained with α_a = .036 which is 25°K above matched load. The deflection above matched load is 4.4 scale divisions giving 5.7°K per scale division as the calibration constant. As most of the data falls near the first calibration point we adopt 6.7°K per scale division as the calibration constant.

All the antenna measurements were made with α_A = .141, thus equation (6-4) becomes

$$T_a = 2(T_3 - 265°K) \tag{6-5}$$

From 1445 EST to 1610 EST on July 21, T_3 is about 304°K corresponding to an antenna temperature of 78°K. At 1610 EST the antenna temperature rises to about 106°K and remains practically constant until 1700 EST after which it drops slowly to its former value.

To summarize, T_a is about 78°K from 1500 EST to 1600 EST, rises to 106°K where it remains for 1 hour, then drops slowly to its former value.

b). Calculations at 1200 Mc (L-Band Radiometer)

The simplified block diagram for the L-Band Radiometer is shown in Figures 6-2, and the pertinent data are given in Table 6-2.

Symbol	Decibels	Power ratio
α_1	2.7	.537
α_2	.2	.955
α_3	.1	.977
α_4	.7	.851
α_5	10.0	.100
α_6	5.6	.280

Table 6-2. Constants of L-Band Radiometer.

Again let T_o be the ambient temperature of the equipment, T_n the effective temperature of the noise source, and T_a the antenna temperature. T_n is 10,000°K and T_o we take as 290°K.
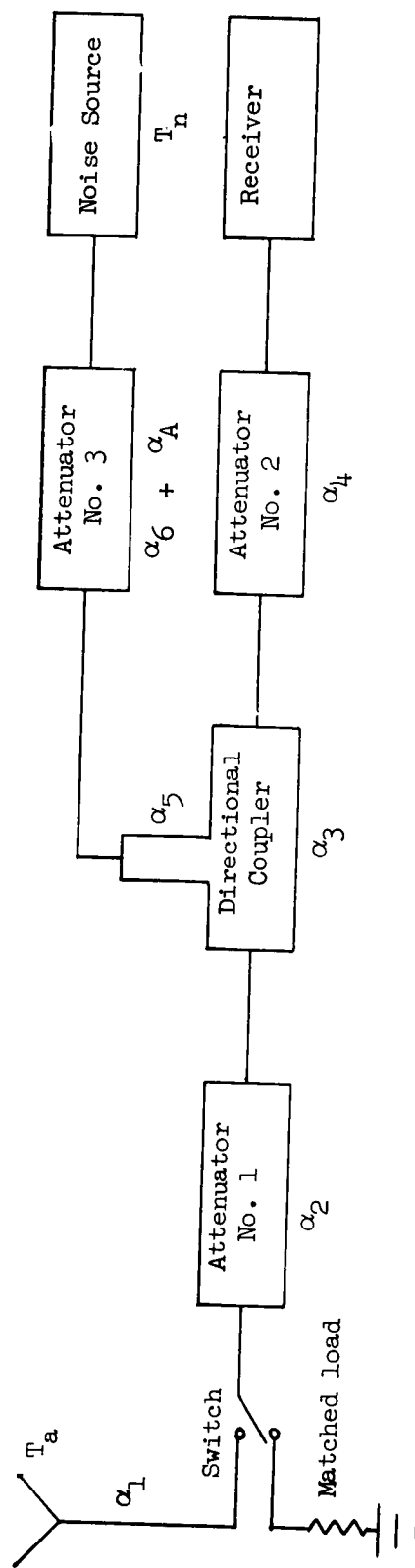
Figure 6-2. Equivalent block diagram of L-Band Radiometer.

With this receiver the calibration procedure is to switch to matched load with the noise source off whereupon the receiver sees the temperature

$$T_1 = \left[T_0 \, \alpha_2 \, \alpha_3 + T_0(1-\alpha_2\alpha_3) + T_0 \, \alpha_6 \, \alpha_a \, \alpha_5 \right.$$
$$\left. + T_0(1-\alpha_6\alpha_a) \, \alpha_5 \right] \alpha_4 + T_0(1-\alpha_4) \tag{6-6}$$

$$T_1 = 315^\circ K$$

The noise source is now turned on giving a temperature,

$$T_2 = \left\{ \left[T_n\alpha_6\alpha_a + (1-\alpha_6\alpha_a) \, T_0 \right] \alpha_5 + T_0 \right\} \alpha_4 + (1-\alpha_4) \, T_0$$

$$T_2 = 231^\circ K \, \alpha_a + 315^\circ K \tag{6-7}$$

To measure antenna temperatures the switch is put in the antenna position and the noise level is adjusted by means of the variable attenuator until the noise level is near the matched load level. In this case

$$T_3 = \left\{ \left[T_a\alpha_1\alpha_2\alpha_3 + T_0(1-\alpha_1\alpha_2\alpha_3) \right] + \left[T_n\alpha_6\alpha_a + (1-\alpha_6\alpha_a) \, T_0 \right] \alpha_5 \right\} \alpha_4$$
$$+ (1-\alpha_4) \, T_0 \tag{6-8}$$

or

$$T_a = 2.34 \, (T_3 - 231^\circ K\alpha_a - 192^\circ K) \tag{6-9}$$

Referring to the data for July 21 we find two calibration points in addition to the matched load level. The first point corresponds to an attenuation of .10 which gives $T_2 = 338^\circ K$ or $23^\circ K$ above matched load. This temperature corresponds to 3.2 scale divisions above matched load for a calibration constant of $7.2^\circ K$ per scale division. The second calibration point is $48^\circ K$ above matched load. With a scale reading of 6.7 we obtain a calibration constant of $7.2^\circ K$ per scale division.

On the chart for July 21, α_a was .446 thus

$$T_a = 2.34 \, (T_3 - 295^\circ K) \tag{6-10}$$

From 1500 EST to 1600 Est on July 21, T_3 is $308^\circ K$ giving an antenna temperature of $30^\circ K$. At 1600 EST the temperature rises abruptly until $T_3 = 318^\circ K$ or $T_a = 54^\circ K$. From 1600 EST to 1700 EST T_a stays constant at $54^\circ K$. At 5 PM T_a drops slowly to its earlier value of $30^\circ K$, after which it remains constant.

c). Calculations at 5 Mc

The chart record for 5 Mc is calculated in microvolts, i.e. a signal generator produces a calibration signal given in microvolts. The corresponding deflection on the chart is noted and a calibration curve can be plotted. Such a curve is shown in Figure 6-3 where the scale reading is plotted against the calibration signal in microvolts. This data was taken from the July 24, 5 Mc record.

To compute the corresponding temperature we use the relation

$$\left[\overline{(E^2)} \right]^{\frac{1}{2}} = \left(4RKT\Delta f \right)^{\frac{1}{2}} \tag{6-11}$$

where $\sqrt{\overline{(E^2)}}$ is the root mean square voltage across the transmission line impedence R, T is the temperature and Δf is the bandwidth of the receiver. For this system R = 50 ohms and Δf = 1000 cps. Taking room temperature at 297°K we find the matched load voltage to be

$$\left[\overline{(E^2)} \right]^{\frac{1}{2}} = \left(4RKT\Delta f \right)^{\frac{1}{2}} = 2.83 \times 10^{-8} \text{ volts} \tag{6-12}$$

To find the temperature T for signals other than matched load we divide equation (6-11) by (6-12) to obtain

$$T = 297 \frac{E^2}{(2.83 \times 10^{-8})^2} \tag{6-13}$$

To find any temperature on the record for July 21, we note the scale reading, find the corresponding microvolt value from Figure 6-3, and use equation (6-13) to find T. Figure (6-4) shows T_a as a function of time for the 5 Mc gear on July 21, 1962. The data for this graph was obtained from the chart record.

d). Calculations at 10 Mc

The 10 Mc data was obtained in tabular form and gave the scale deflection in microvolts for each hour on July 21, 1962. Using this data and equation (6-13) derived in the preceding section a graph of T_a vs. time is plotted. This graph is shown in Figure (6-5). The data for this graph was obtained by averaging the hourly values for all the days of July, and finding the hourly departures for each day. Thus it actually shows the temperature increase over an average day.

e). Calculations at 224 Mc

Temperature reductions for 224 Mc were made by Mr. Straka. These may
be summarized as follows: From 1500 EST to 1600 EST the antenna temperature
remains about constant in the 450-550°K range with a slight maximum at
1545 EST. At 1610 EST the temperature rises suddenly to about 600°K and
remains almost constant until 1715 EST, after which it drops slowly. At
1800 EST the temperature goes through a sharp minimum and drops to 400°K.
It then rises quickly until it again becomes 600°K at 1830 EST. The antenna
temperature then drops slowly to the point where the record ends at 1946 EST.

f). Discussion of Antenna Temperatures

Thus far in the reduction of the temperatures we have neglected such
things as background sky radiation, ground effects, beamwidth etc. We now
proceed to discuss these factors and attempt to make a reasonable estimate
of the temperature in the storm cell.

1). 1200 Mc and 3000 Mc

For these frequencies the size of the cell was large compared to the
beamwidth. Thus the antenna temperatures will be given by equation (3-1).
At both 1200 and 3000 Mc the storm cell observations were made at 7° elevation
and as the antenna moved to this position a temperature rise of about 25°K
occurred. Later measurements show that the sky temperature was about the
same at this elevation without a storm. Hence we conclude that there is no
significant radiation from this particular storm cell at 1200 and 3000 Mc
other than that from lightning strokes.

2). 224 Mc

Again, we use equation (3-1) as the storm cells fill the beam at this
particular frequency. When the normal sky temperature for this frequency
(Kraus and Ko, 1957) is subtracted from the observed antenna temperatures we
obtain values of T_b in the range of 300°K to 500°K. If we assume a maximum
value of τ, the optical depth, equal to 10^{-2}, (see section 4-d), brightness
temperatures in the range $30,000^{\circ}$K to $50,000^{\circ}$K are obtained for the brightness
temperatures in the cell.

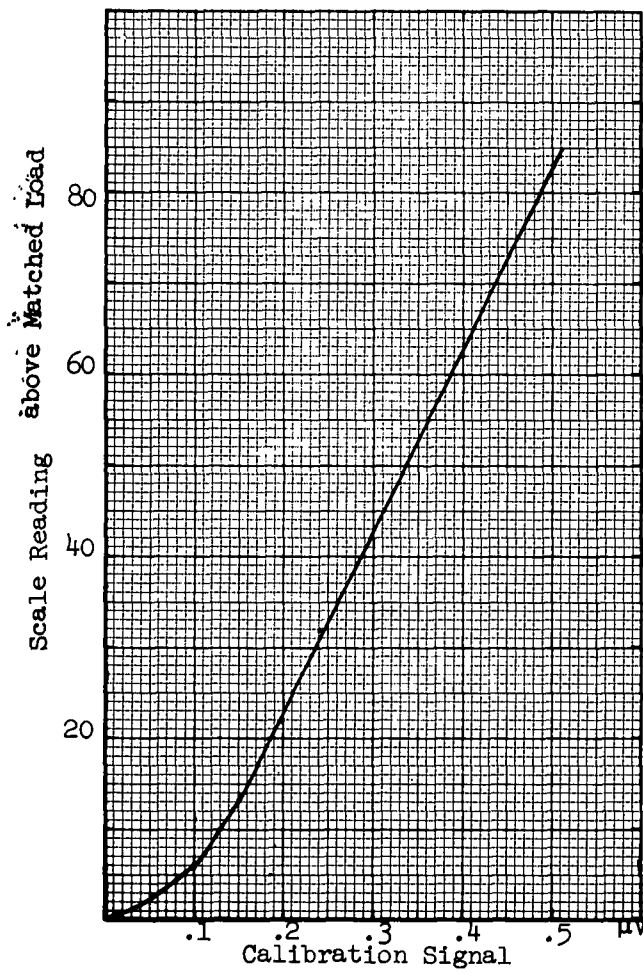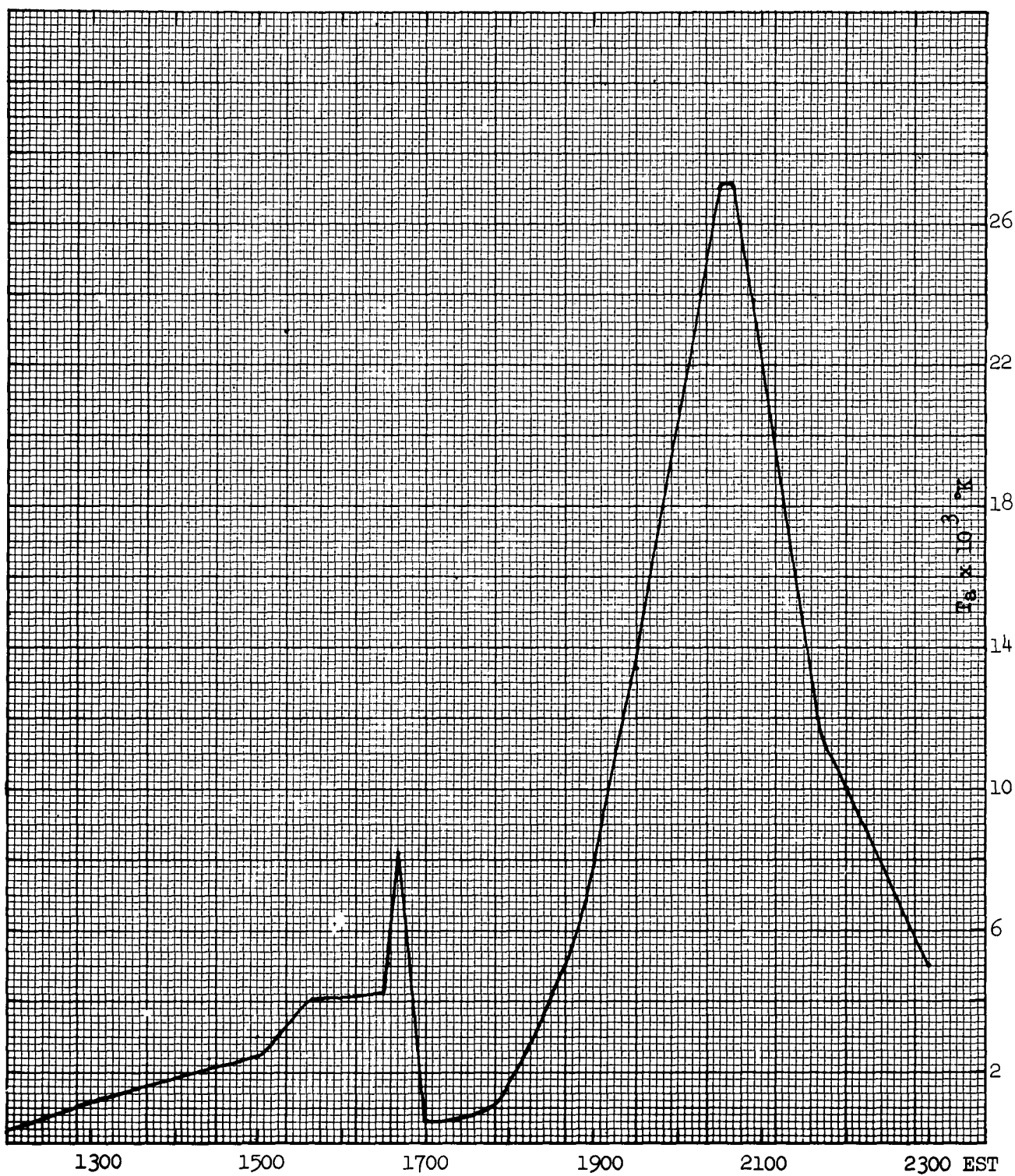Figure 6-3   Calibration Curve for 5 Mc.
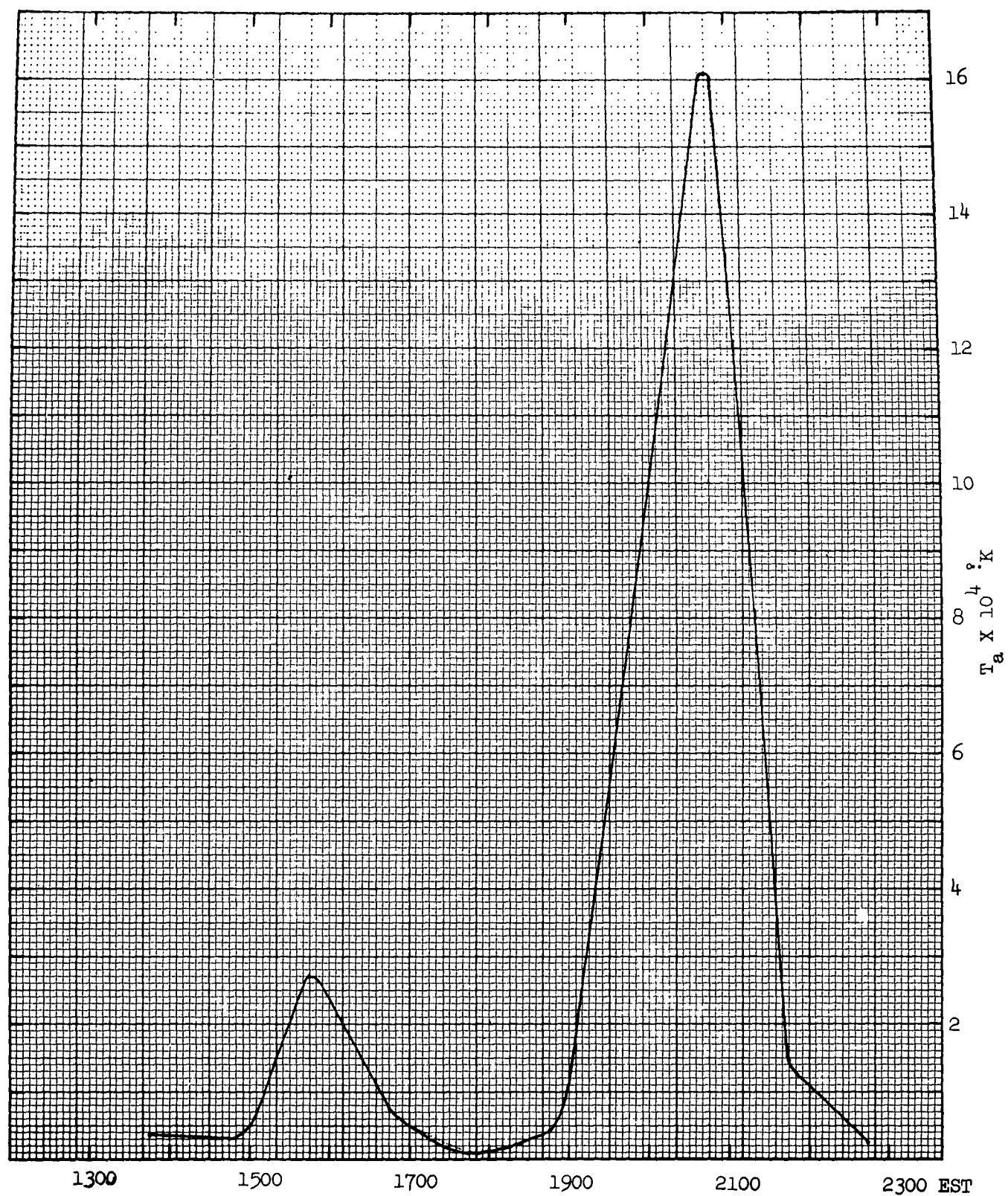
Figure 6-4.   Antenna Temperature at 5 Mc.

Figure 6-5. Antenna Temperature at 10 Mc.

3). 30 Mc

No reductions were attempted at 30 Mc as the receiver data was incomplete as this report was being made. A qualitative idea of the behavior of the radiation from the cell at 30 Mc can be obtained from the graph of 30 Mc radiation which appears in Figure 2-4.

4). 10 Mc

At 10 Mc we neglect all ground effects. The antenna was a dipole and for our purposes we will assume it had an isotropic radiation patterns. The tabulated data consisted of average signal levels for each day and hour in July, and the departures from this average for each day and hour.

Thus we assume any diurnal variation in the signal level has been averaged out and the departure for the particular day and hour of the storm can be attributed directly to the effects of the storm. Referring to Figure (6-5) it is seen that at 1615 EST the first storm reached its maximum intensity with an antenna temperature of about $30,000^\circ$K. Assuming the storm was some 10 km. away and had an effective area of about 100 square km. we find that its black body temperature is

$$T = \frac{4\pi T_a}{\frac{100}{10^2}} = 3.8 \times 10^5 \; {}^\circ K$$

At 2045 EST violent weather conditions, including lightning and rain, were in the immediate area of the site. In this case we may assume the storm fills the antenna beam and that the antenna temperature is identical to the temperature in the storm. This gives a temperature of $1.6 \times 10^5 \; {}^\circ$K. This temperature differs by a factor of about 2 from the temperature calculated above. Thus we obtain a mean temperature of $2.7 \times 10^5 \; {}^\circ$K at 10 Mc.

5). 5 Mc

Considering the location of the storm and the directivity of the antenna, little error results in assuming an isotropic radiation pattern for the antenna. With the same assumptions used in the 10 Mc calculations we find

$$T = 1 \times 10^5 \; {}^\circ K,$$

where we have used 8000°K as the antenna temperature for the first observation of the storm.

Following the same arguments as above for the storm at 2045 EST we obtain a temperature of 2.7×10^4 °K. This temperature differs by about a factor of four from the temperature obtained at 1615 EST. The two temperatures give a mean temperature of 6.4×10^4 °K at 5 Mc.

7. Evaluation of the Parameters of the corona discharge model

In evaluating expression (5-7) for the equivalent températures of the cells, the values of B, τ and β in equation (5-2), the length L of the discharge, the number of discharges n per unit volume per second and the size of the total volume must be known. For B, τ and β the values given by Heintz or those corresponding to the waveform observed by Denholm can be employed. Also these values of B, τ and β are used in the calculation of the total radiated power by equation (5-5). But the accuracy of these values for observed waveforms is limited by the equipment and methods employed in the observations. Also, the situation in the corona discharge of the charged particles in the atmosphere and the metal point may be different.

a). Temperature Estimates Using Heintz's Data

The values of B, τ and β given by Heintz for the point to plane corona discharge which are shown in Section 5 are employed in the following calculations. Also the following numerical assumptions were made.

$$L = 3 \times 10^{-3} \text{ meter}$$

$$V = \pi R_s^3 = \pi (500)^3 \quad \text{meter}^3$$

where R_s (radius of the source) = 500 m and a spherical volume is assumed.

It is known (Gunn 1957, Schonland 1953) that in one lightning discharge the average amount of charge is around 20 coulombs, and this charge is built up in 5 seconds in severe storms. If it is assumed that the amount of charge involved in the corona discharge is of the same order of magnitude and also that one discharge involves 0.1 e.s.u. (Gunn 1958), then the number of discharges per second is

$$\frac{20 \text{ (coulombs)}}{5 \times 3.336 \times 10^{-11}} = 1.2 \times 10^{11} \text{ discharges sec}^{-1}$$

$$= n V$$

The value of n becomes 3.06×10^2 discharges $\text{sec}^{-1} \text{ m}^{-3}$.

Using these values, the calculation of the equivalent temperature T_b is made by equation (5-7). The results are shown as T_b (1) in Table 7-1 (a) and in Figure 7-1.
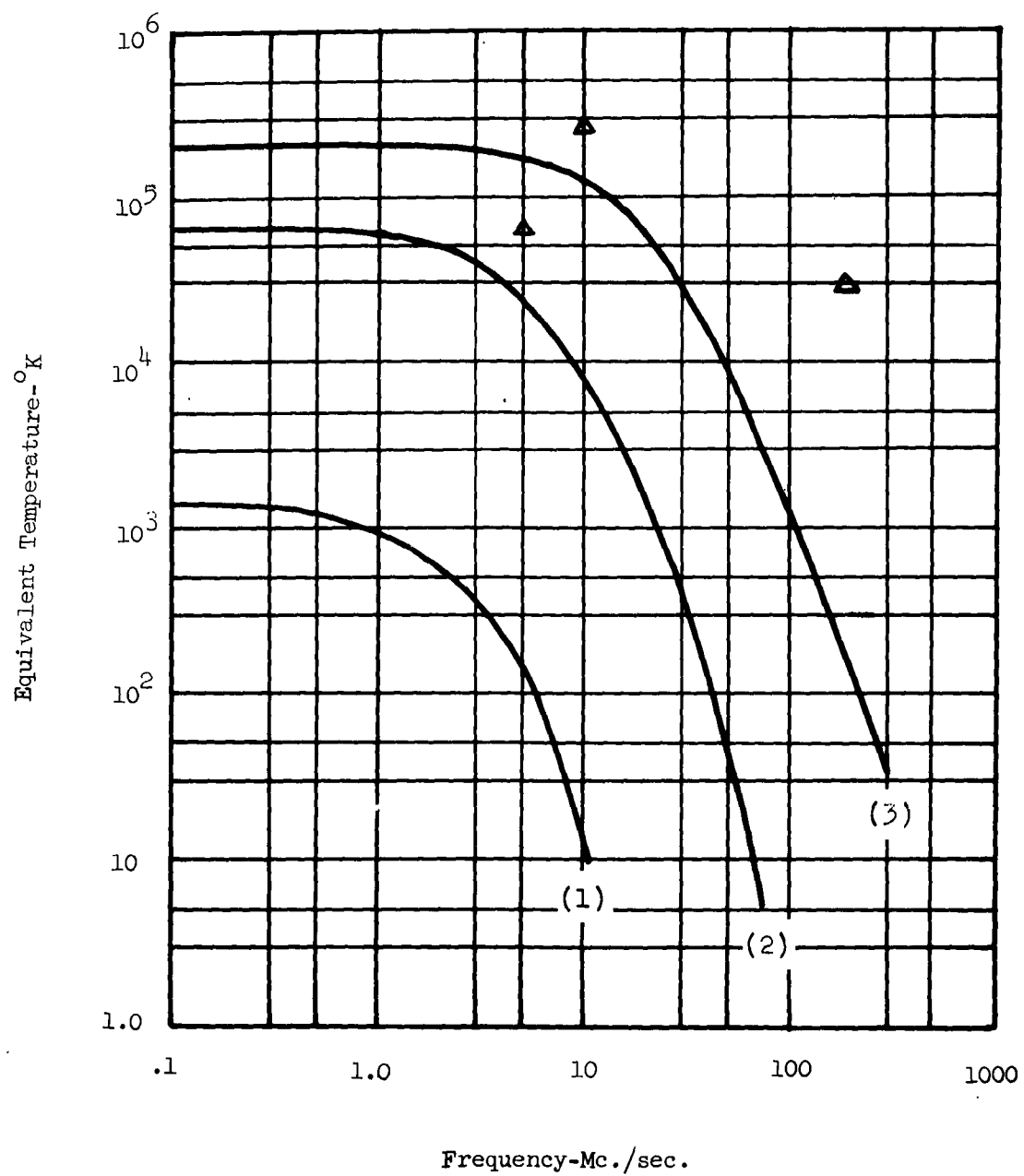
Figure 7-1. Theoretical Relation between Temperature T_b and Frequency. △ refer to observed values from Section 6.

Table 7-1(a) Calculated Temperature

Frequency (Mc)	$T_b(1)$(Heintz) °K	$T_b(2)$(Denholm) °K	$T_b(3)$(Denholm) °K
0.1	1370	6.4×10^4	1.97×10^5
0.3	1310	6.27×10^4	1.97×10^5
1.0	873	6.02×10^4	1.95×10^5
3.0	390	4.05×10^4	1.93×10^5
10	12.7	8.77×10^3	1.31×10^5
30		4.23×10^2	2.84×10^4
100		9.1×10^1	1.49×10^3
200			2.91×10^1
300			2.9×10^0

Table 7-1(b) Parameters Used in the Calculation

	(1)	(2)	(3)
B (Amp. sec $^{3/2}$)	2.61×10^{-14}	3.34×10^{-13}	3.34×10^{-14}
τ (sec)	11.8×10^{-8}	4.0×10^{-8}	1.3×10^{-8}
β (sec $^{-1}$)	4.82×10^6	14.5×10^6	45×10^6

The radiated power is also calculated for the above parameters by equation (5-5) and shown in Figure 7-2.

b). Temperature Estimates Using Denholm's Data

Denholm observed the current wave forms of Trichel pulses of the metal point to metal plate corona discharge with a high speed oscilloscope (Denholm 1960). From the observed wave form, the values of B, τ and β to be employed in the calculation are estimated as shown in Table 7-1 (b).

With these values, the charge in one pulse becomes about 1 e.s.u. instead of 0.1 e.s.u. and then the number of discharges per second becomes

$$n \, V = 1.2 \times 10^{10}$$

Using the same values for L and R_s as in the preceding case, the equivalent temperatures are calculated and shown as $T_b(2)$ in Table 7-1 (a).

If instead of increasing the amount of charge to 1 e.s.u., the value of B is decreased to keep this charge at 0.1 e.s.u. the equivalent temperature becomes 1/10 of the value listed as T_b (2).

c). Temperature Estimates Using Other Values of the Parameters.

In case (2), the values of B, τ, and β are taken from the wave form of a typical Trichel pulse observed by Denholm. But, he shows that there is a wide range of observed rise times, ranging from 0 to 20 milli micro seconds after corrections. Also the rise time of the oscilloscope was 6 milli micro seconds and with this value the faster pulses cannot be observed effectively. We have tried a calculation for a hypothetical pulse shape with a faster rise and fall time than case (2). The values employed are indicated in Table 7-1 (b) and results are shown as T_b (3) in Table 7-1 (a).

From the values of Table 7-1 (a), it is seen that the calculated temperature change markedly with the selection of the parameters. The values of $T_b(1)$ are rather small. Possibly this may be explained if the high frequency component is not well represented in the measurements by Heintz because of his instrumental limitations.
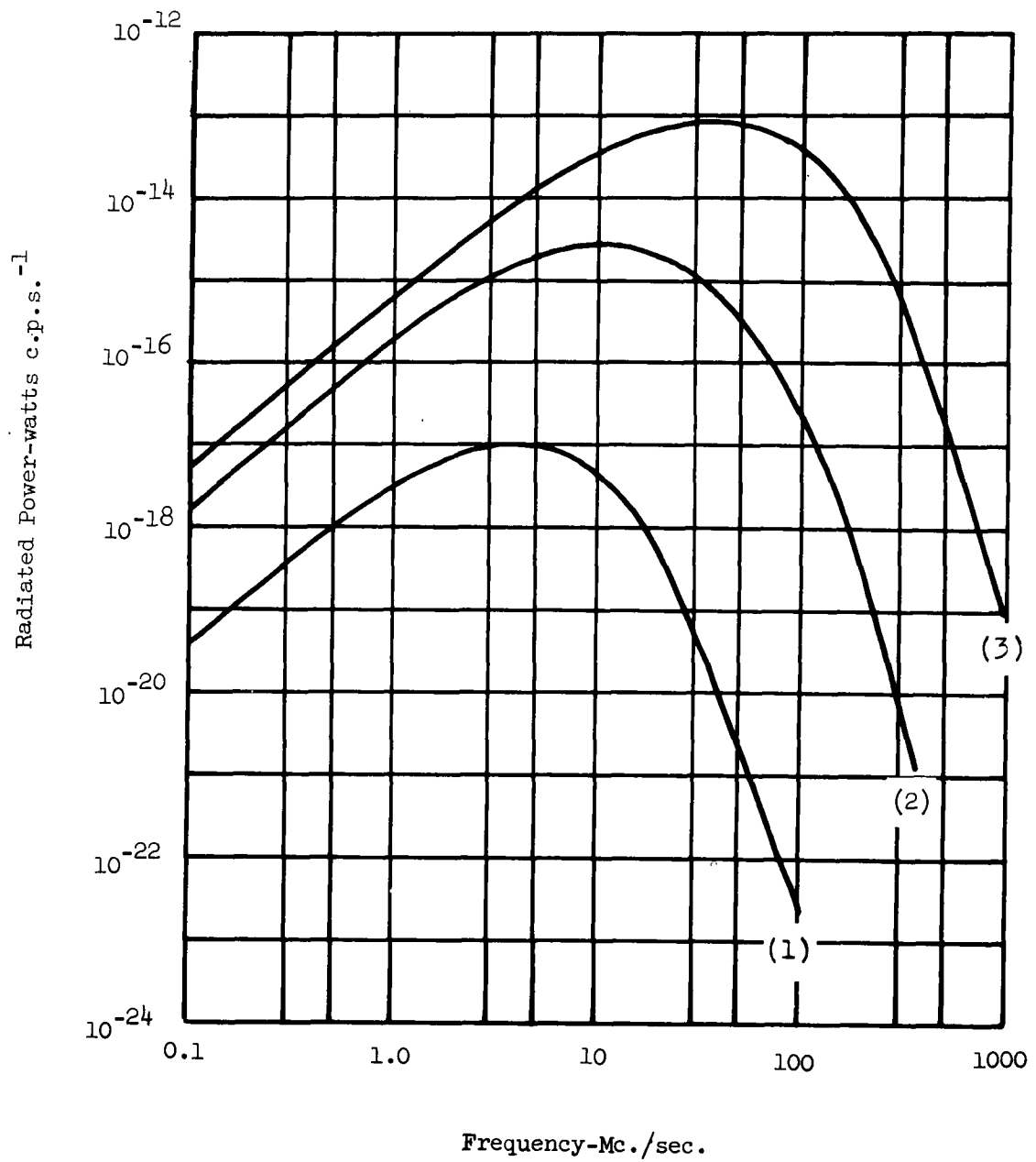
Figure 7-2.   Theoretical Relation between Radiated Power and Frequency.

In the actual corona discharge in the atmosphere, it is expected that there are wide variations in the charge per particle, and the actual power spectrum or the equivalent temperature must be the superposition of the effects of various sizes of the discharge, i.e. over various amounts of charge and various amounts of rise and fall time of the discharge. Then the peak of the radiation spectrum will become much more broad and the decrease of the equivalent temperature in high frequencies will be much slower than in the case of uniform pulse shapes assumed in our three cases.

Figure 7-1 shows in addition to the theoretical curves derived in this section points representing the observed temperatures found in section 6.

8. Discussion

The foregoing analysis was made using a single wave form and uniform charge for each discharge. However, the actual conditions in a thunderstorm cell must include a wide dispersion of wave forms as well as a large variation of particle charges. The total, uniform charge on each particle of 0.1 or 1 esu. was an assumption based on meteorological measurements of raindrops which reach the earth. To our knowledge, no measurement of drop charges in an active thunderstorm cell have been made, and whether ground-measured charges correspond exactly with these existing in the upper regions of a storm cloud is not known at present. Indeed, the very mechanism for electrification of the drops is the subject of some controversy.

Although only corona discharge was analysed as the principal emission mechanism, several other effects must be discussed. Thermal emission is considered negligible as the opacity of the cell is quite small. Discharges from objects on the surface of the earth, e.g. trees, antennas, buildings, etc., would certainly produce detectable radiation, though no measurements were made of these contributions alone. Also, charged drops of water, striking the surface of the earth, will produce a certain amount of radiation which was integrated with all other effects in the measurement. The exact quantitative contribution of this mechanism is not known.

At 5 Mc the effect of other centers of activity producing radio-frequency radiation (not necessarily thunderstorms) must be considered. This is due to the total-refraction effect of the F-layer of the ionosphere at this frequency. Ionospheric soundings for July 21, 1961 taken at Millstone Hill, Massachusetts indicate a mean maximum-usable frequency for the period 1530 EST to 2330 EST at 5.0 Mc.

Dr. A. P. Mitra suggested this effect to us in a private communication and feels that sources up to a distance of 2000 km. could be seen at this frequency due to the total-refraction. Hence the values of 5 Mc noise intensity should be considered a maximum value for this storm and are probably lower for the cell emission, per se. The fact that values of intensity for this frequency were obtained as difference measurements from the record for July 18, 1961 should help correct for this effect but no quantitative estimates can be given.

Depending on the angle of incidence at the ionosphere, frequencies as high as 10 Mc could be affected in this manner. However, the effect diminishes rapidly with increasing frequency. Also, the values of intensity used in this report for the July 21, 1961 event at 10 Mc were obtained as the difference in intensity for this date from the monthly mean at 1615 EST and 2045 EST. Thus, propagation effects should have a minimum effect on the intensity as it is doubtful if thunderstorms were present in the affected area every day of the month of July.

Considering the approximations necessarily made in the preceding sections and the uncertain observational corrections described above, the intensity measurements plotted on Figure 7-1 should be understood as maximum values, and may be too high by an order of magnitude, or more. Unfortunately, this means that they cannot be used to distinguish the mechanisms considered in Section 7.

Further investigations of radio-frequency emission from thunderstorm cells should be conducted in such a manner that some or all of the observational errors mentioned above can be corrected or at least accounted for. This would, of course, include improved meteorological data in order to allow the formulation of a better theoretical basis for comparison with the observations.

The measured temperature at L and S band are very small and this is consistent with the simple theory outlined in this report. But to obtain more definite values of the temperatures, it would be necessary to improve the calibration methods, to obtain more accurate background temperatures, and to check the constancy of antenna impedance.

Some suggested precautions for measurements at these frequencies are described in sections (10) and (11).

A possible application of this observed effect of thunderstorm emission is the passive determination of cell position by triangulation methods. This could of course also make use of the lightning discharges, and indeed one cell was found this way prior to its detection by the radar observers.

9. Effect of Radiation from the Ground and the Atmosphere

When the antenna gain function is $G(\Omega)$ where Ω is the solid angle which is referred to the antenna, the antenna temperature becomes

$$T_A = \int_{4\pi} G(\Omega)\, T(\Omega)\, d\Omega \tag{9-1}$$

The integration is made over the whole sphere, 4π . $T(\Omega)$ is the distribution of the brightness temperature of sky and ground seen from the antenna.

In Figure 9-1 a typical distribution of $T(\Omega)$ is shown. In the solid angle occupied by the ground, $T(\Omega)$ will be about that of the actual ground temperature but it will be different for populated areas and depends on meteorological conditions.

Also $T(\Omega)$ may have a considerable value above the ground due to atmospheric absorption. One example of its measurement is given by Mezger (1959). In this article the dependence of $T(\Omega)$ on the geography is also observed.

It is usually considered that a considerable fraction of the total energy goes out in the main beam of an antenna when it is employed as a transmitting antenna. We may write

$$\int_{\text{main beam}} G(\Omega)\, d\Omega = \eta \tag{9-2}$$

and
$$\int_{\substack{\text{side lobes} \\ \text{spill over}}} G(\Omega)\, d\Omega = 1-\eta \tag{9-3}$$

The values of η in these expressions are of the order of tens of percent. This factor may be called the quality factor of an antenna.
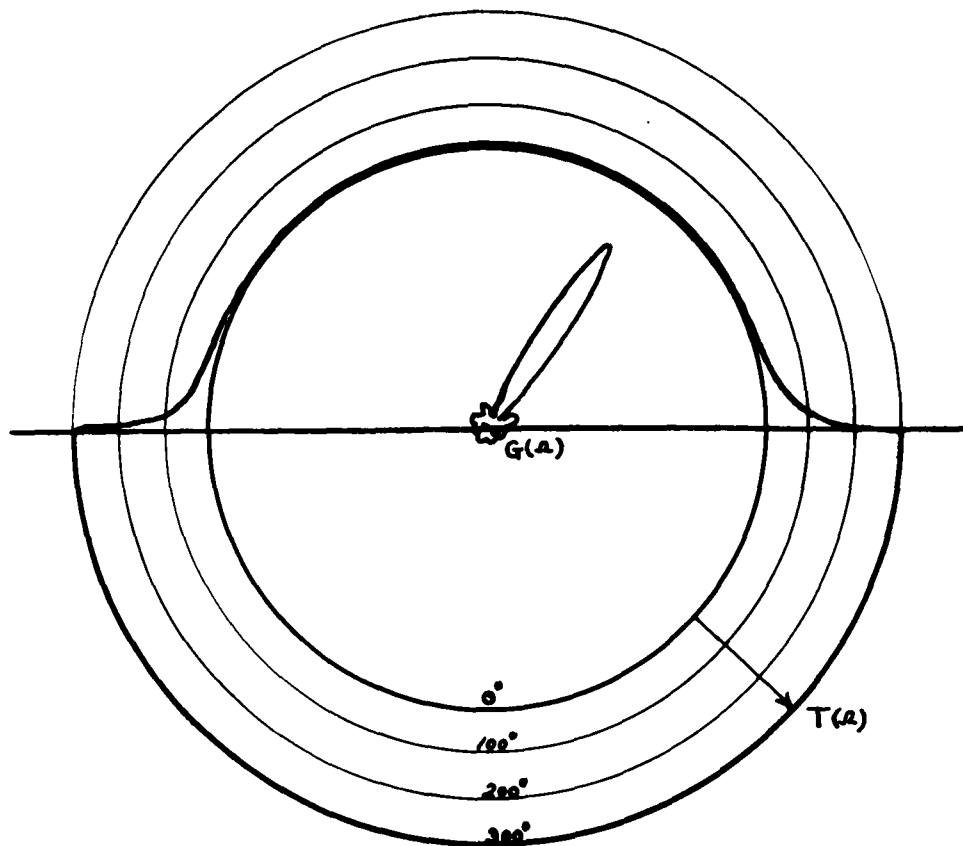
Figure 9-1.   Temperature Distribution around Antenna.

The distribution of the side lobes and spill over is complicated, and depends on the illumination on the parabolic surface and the design of the primary feed. When the antennas main beam is directed to a portion of the sky with temperature $T_s(\Omega)$

$$T_A = \int_{\text{main beam}} G(\Omega) \; T_s(\Omega) \; d\Omega$$

main beam

$$+ \int_{\text{side lobes}} G(\Omega) \; T_G(\Omega) \; d\Omega$$

(9-4)

side lobes

spill over

where $T_G(\Omega)$ is the temperature distribution in the angle not occupied by the main beam. Because of the fact that the ground and the portion of the sky which has considerable temperature due to the atmospheric absorption occupies more than half the total solid angle, the contribution to T_A from the second term of the above expression becomes considerable. This contribution depends on the behavior of $G(\Omega)$ in the direction of side lobes and spill over. Generally when the quality factor η is large, this contribution is small and for the same η it can be small if the backward spill over is small when the elevation of the main beam is high. The contribution from the second term may range from $10^\circ K$ to $100^\circ K$. At present, the antenna with the least antenna temperature is the special low noise form developed by Bell Telephone laboratories with about $4.5^\circ K$ and 5650 Mc (Grasse 1959).

As the object of the radio measurement is to determine the first term of equation (9-4), it is necessary to make the effect of the second term as small as possible, especially when it is desired to detect a small variation of the first term. The second term cannot be assumed to stay constant even when the antenna main beam direction is fixed, because it is affected by variable man-made noise and meteorological conditions. When low noise type receivers, such as masers and parametoric amplifiers, are used, this term is the main factor limiting the sensitivity of the system.

At present, it is considered to be difficult to obtain reliable radiation pattern characteristic for large antennas. But because of the above considerations, the development of techniques for evaluating the side lobes and spill over of a large antenna would be very important.

10. Effect of Antenna Impedance

In most of the theoretical considerations on the ratio detection technique of the sky temperature, it is assumed that the impedance of the antenna is matched to the input of the receiver and stays constant in this condition. But in actual practice this condition is not fulfilled and the effect of its variation is discussed in the following

The output T_{out} of a receiver can be expressed as

$$T_{out} = A(T_R + T_A) \qquad (10\text{-}1)$$

where T_A is the antenna temperature, T_R is the effective temperature of the receiver, and A is the amplification factor.

When the real component of the impedance of the antenna changes from R_o to $R_o + \Delta R$, T_A changes. Also T_R changes when the input impedance of the receiver is varied. The variation of T_R due to this effect is complicated and it depends on the type of the amplifier or mixer employed in the first stage. Also the amplification A changes due to the input impedance. The output becomes

$$T_{out}' = A'(T_R' + T_A') \qquad (10\text{-}2)$$

for the same antenna setting. The use of the actual T_{out}' in equation (10-1) will result in a false value for T_A.

Usually the guaranteed range of the impedance of the standard connectors is 1.05 in terms of the standing wave ratio and the impedance of the the antenna feeds exposed to the weather can easily change from the matched condition to which they were originally adjusted. An effect on the antenna impedance from near by objects influenced through the side and back lobes is also possible. The use of a circulator between the antenna and the receiver can reduce the variation of T_R and A due to the antenna impedance variation, but cannot prevent the variations of T_A itself.

Because of this effect of antenna impedance, it is necessary to check the antenna impedance frequently in precise measurements.

11. References

Amin, R. A. 1954, J.A.P. 25, 210, 358, 627.

Atlas, D., and Marshall, J.S., et.al. 1952, "Weather Effects on Radar", Air Force Surveys in Geophysics, No. 23, Air Force Cambridge Research Center.

Compen, C. F., Jr., et.al. 1960, Handbook of Geophysics, Revised Ed., MacMillan, New York, 1-16.

DeGrasse, R. W., Hogg, D. C., Ohm, E.E. and Scovil, H. E. 1959, J.A.P. 30, 2013.

Denholm A. S.;1960, Trans. AIEE 79 III, 698.

English, W.W.,1948, Phys. Rev., 74, 170.

Gunn, R., 1957, Proc. IRE 45, 1331.

Gunn, R., 1958, Houghton, H.G. (ed.) Atmospheric Explorations, Wiley and Technology Press, 18 .

Heintz, W., 1959, Z.f.a. Phys. xl, 51.

Hogg, D. C., and Mumford, W. W. 1960, Microwave Journal, March, 80.

Johnson J. C., 1954, Physical Meteorology, John Wiley and Sons, New York, 257.

Johnson J.C., 1955, "Meteorological Factors and Their Effects on Microwave Propagation", Technical Memorandum 412, Hughes Aircraft Co., Culver City, California.

Kraus, J. D., and Kö, H.C. 1957, Celestial Radio Radiation, Scientific Report No. 1, Contract A F 19(604)-1951.

Lichtenstein, P. 1959, Paper presented at the Toronto Meeting of the American Astronomical Society.

Mezger, P. G. 1959, Z.f.a. Phys. xl, 4.

Pawsey, J. L. and Bracewell, R. N. 1955, Radio Astronomy, Oxford.

Schonland, B. F. J., 1953, Atmospheric Electricity, John Wiley and Sons, Inc., N. Y. 61.

Van Vleck, J. H.,1947, Phys. Rev. 71, 413, 427.

Vonnegut, B., 1954, Proceedings on Conference on Atmospheric Electricity, ed. Holzer and Smith., 173, 175; Geophysical Research Papers, No. 42, Air Force Cambridge Research Center.

von Hippel, A. R., ed. 1954, Dielectric Materials and Applications, Wiley, New York, 361.

12. Personnel

Dr. Robert Fleischer, Principal Investigator

Dr. Masakazu Oshima, Research Assistant (from July 1, 1961).

Mr. Raymond E. Falconer, Research Assistant (to Nov. 30, 1961).

Mr. Terry Roark, Graduate Assistant

Mr. Marvin DeJong, Graduate Assistant (from Feb. 1, 1962).

Mr. Ralph Haskell, Technician (to June 30, 1961).